34. Malaspina A, Kaushik N, de Belleroche J: A 14-3-3 mRNA is up-regulated in amyotrophic lateral sclerosis spinal cord. J Neurochem 2000, 75:2511–2520
35. Carpenter MK, Cui X, Hu Z-Y, Jackson J, Sherman S, Seiger Å, Wahlberg LU: In vitro expansion of a multipotent population of human neural progenitor cells. Exp Neurol 1999, 158:262–278
36. Satoh J, Kuroda Y: Differential gene expression between human neurons and neuronal progenitor cells in culture: an analysis of arrayed cDNA clones in NTera2 human embryonal carcinoma cell line as a model system. J Neurosci Methods 2000, 94:155–164
37. Loeb KR Haas AL: Conjugates of ubiquitin cross-reactive protein distribute in a cytoskeletal pattern. Mol Cell Biol 1994, 14:8408–8419
38. Prasad GL, Valverius EM, McDuffie E, Cooper HL: Complementary DNA cloning of a novel epithelial cell marker protein, HME1, that may be down-regulated in neoplastic mammary cells. Cell Growth Differ 1992, 3:507–513
39. Cardoso C, Leventer RJ, Ward HL, Toyo-oka K, Chung J, Gross A, Martin CL, Allanson J, Pilz DT, Olney AH, Mutchinick OM, Hirotsune S, Wynshaw-Boris A, Dobyns WB, Ledbetter DH: Refinement of a 400-kb critical region allows genotypic differentiation between isolated lissencephaly, Miller-Dieker syndrome, and other phenotypes secondary to deletions of 17p13.3. Am J Hum Genet 2003, 72:918–930
40. Toyo-Oka K, Shinoya A, Gambello MJ, Cardoso C, Leventer R, Ward HL, Ayala R, Tsai L-H, Dobyns W, Ledbetter D, Hirotsune S, Wynshaw-Boris A: 14-3-3ε is important for neuronal migration by binding to NUDEL: a molecular explanation for Miller-Dieker syndrome. Nat Genet 2003, 34:274–285
41. Konishi H, Nakagawa T, Harano T, Mizuno K, Saito H, Masuda A, Matsuda H, Osada H, Takahashi T: Identification of frequent G_2 checkpoint impairment and a homozygous deletion of 14-3-3ε at 17p13.3 in small cell lung cancers. Cancer Res 2002, 62:271–276
42. Kimura MT, Irie S, Shoji-Hoshino S, Mukai J, Nadano D, Oshimura M, Sato T-A: 14-3-3 is involved in p75 neurotrophin receptor-mediated signal transduction. J Biol Chem 2001, 276:17291–17300
43. Won J, Kim DY, La M, Kim D, Meadows GG, Joe CO: Cleavage of 14-3-3 protein by caspase-3 facilitates Bad interaction with Bcl-x(L) during apoptosis. J Biol Chem 2003, 278:19347–19351
44. Conklin DS, Galaktionov K, Beach D: 14-3-3 proteins associate with cdc25 phosphatases. Proc Natl Acad Sci USA 1995, 92:7892–7896
45. Wang X, Grammatikakis N, Siganou A, Calderwood SK: Regulation of molecular chaperone gene transcription involves the serine phosphorylation, 14-3-3ε binding, and cytoplasmic sequestration of heat shock factor 1. Mol Cell Biol 2003, 23:6013–6026
46. Alam R, Hachiya N, Sakaguchi M, Kawabata S-I, Iwanaga S, Kitajima M, Mihara K, Omura T: cDNA cloning and characterization of mitochondrial import stimulation factor (MSF) purified from rat liver cytosol. J Biochem 1994, 116:416–425
47. Chan TA, Hermeking H, Lengauer C, Kinzler KW, Vogelstein B: 14-3-3σ is required to prevent mitotic catastrophe after DNA damage. Nature 1999, 401:616–620
48. Hermeking H, Lengauer C, Polyak K, He T-C, Zhang L, Thiagalingam S, Kinzler KW, Vogelstein B: 14-3-3σ is a p53-regulated inhibitor of G2/M progression. Mol Cell 1997, 1:3–11
49. Ferguson AT, Evaron E, Umbricht CB, Pandita TK, Chan TA, Hermeking H, Marks JR, Lambers AR, Futreal PA, Stampfer MR, Sukumar S: High frequency of hypermethylation at the 14-3-3 σ locus leads to gene silencing in breast cancer. Proc Natl Acad Sci USA 2000, 97:6049–6054
50. Dellambra E, Golisano O, Bondanza S, Siviero E, Lacal P, Molinari M, D'Atri S, De Luca M: Downregulation of 14-3-3σ prevents clonal evolution and leads to immortalization of primary human keratinocytes. J Cell Biol 2000, 149:1117–1129
51. Mucke L, Eddleston M: Astrocytes in infectious and immune-mediated diseases of the central nervous system. EMBO J 1993, 7:1226–1232
52. Ridet JL, Malhotra SK, Privat A, Gage FH: Reactive astrocytes: cellular and molecular cues to biological function. Trends Neurosci 1997, 20:570–577
53. Bush TG, Puvanachandra N, Horner CH, Polito A, Ostenfeld T, Svendsen CN, Mucke L, Johnson MH, Sofroniew MV: Leukocyte infiltration, neuronal degeneration, and neurite outgrowth after ablation of scar-forming, reactive astrocytes in adult transgenic mice. Neuron 1999, 23:297–308
54. Menet V, Ribotta MGY, Chauvet N, Drian MJ, Lannoy J, Colucci-Guyon E, Privat A: Inactivation of the glial fibrillary acidic protein gene, but not that of vimentin, improves neuronal survival and neurite growth by modifying adhesion molecule expression. J Neurosci 2001, 21:6147–6158
55. Yamada T, Kawamata T, Walker DG, McGeer PL: Vimentin immunoreactivity in normal and pathological human brain tissues. Acta Neuropathol 1992, 84:157–162
56. Holley JE, Gveric D, Newcombe J, Cuzner ML, Gutowski NJ: Astrocyte characterization in the multiple sclerosis glial scar. Neuropathol Appl Neurobiol 2003, 29:434–444
57. Galou M, Solucci-Guyon E, Ensergueix D, Ridet J-L, Robotta MGY, Privat A, Babinet C, Dupouey P: Disrupted glial fibrillary acidic protein network in astrocytes from vimentin knockout mice. J Cell Biol 1996, 133:853–863
58. Eliasson C, Sahlgrens C, Berthold C-H, Stakeberg J, Celis JE, Betsholtz C, Eriksson JE, Pekny M: Intermediate filament protein partnership in astrocytes. J Biol Chem 1999, 274:23996–24006
59. Pekny M, Johansson B, Eliasson C, Stakeberg J, Wallén Å, Perlmann T, Lendahl U, Betsholtz C, Berthold C-H, Frisén J: Abnormal reaction to central nervous system injury in mice lacking glial fibrillary acidic protein and vimentin. J Cell Biol 1999, 145:503–514
60. Inagaki M, Nakamura Y, Takeda M, Nishimura T, Inagaki N: Glial fibrillary acidic protein: dynamic property and regulation by phosphorylation. Brain Pathol 1994, 4:239–243
61. Nicholl ID, Quinlan RA: Chaperone activity of α-crystallins modulates intermediate filament assembly. EMBO J 1994, 13:945–953
62. Lopez-Egido JR, Cunningham J, Berg M, Oberg K, Bongcam-Rudloff E, Gobl AE: Menin's interaction with glial fibrillary acidic protein and vimentin suggests a role for the intermediate filament network in regulating menin activity. Exp Cell Biol 2002, 278:175–183
63. Chen XQ, Yu ACH: The association of 14-3-3γ and actin plays a role in cell division and apoptosis in astrocytes. Biochem Biophys Res Commun 2002, 296:657–663
64. Chen XQ, Chen JG, Zhang Y, Hsiao WWL, Yu ACH: 14-3-3γ is upregulated by in vitro ischemia and binds to protein kinase Raf in primary cultures of astrocytes. Glia 2003, 42:315–324
65. Tzivion G, Luo Z-J, Avruch J: Calyculin A-induced vimentin phosphorylation sequesters 14-3-3 and displaces other 14-3-3 partners in vivo. J Biol Chem 2000, 275:29772–29778
66. Tsujimura K, Tanaka J, Ando S, Matsuoka Y, Kusubata M, Sugiura H, Yamauchi T, Inagaki M: Identification of phosphorylation sites on glial fibrillary acidic protein for cdc2 kinase and Ca^{2+}-calmodulin-dependent protein kinase II. J Biochem 1994, 116:426–434
67. Goto H, Kosako H, Tanabe K, Yanagida M, Sakurai M, Amano M, Kaibuchi K, Inagaki M: Phosphorylation of vimentin by Rho-associated kinase at a unique amino-terminal site that is specifically phosphorylated during cytokinesis. J Biol Chem 1998, 273:11728–11738
68. Takemura M, Gomi H, Colucci-Guyon E, Itohara S: Protective role of phosphorylation in turnover of glial fibrillary acidic protein in mice. J Neurosci 2002, 22:6972–6979
69. Goto H, Yasui Y, Kawajiri A, Nigg EA, Terada Y, Tatsuka M, Nagata K-I, Inagaki M: Aurora-B phosphorylates the cleavage furrow-specific vimentin phosphorylation in the cytokinetic process. J Biol Chem 2003, 278:8526–8530
70. Masters SC, Fu H: 14-3-3 proteins mediate an essential anti-apoptotic signal. J Biol Chem 2001, 276:45193–45200

ELSEVIER

Journal of Autoimmunity 23 (2004) 293–300

journal of autoimmunity

www.elsevier.com/locate/issn/08968411

Synthetic glycolipid OCH prevents insulitis and diabetes in NOD mice

Miho Mizuno[a], Makoto Masumura[a], Chiharu Tomi[a], Asako Chiba[a,b], Shinji Oki[a], Takashi Yamamura[a], Sachiko Miyake[a,*]

[a]*Department of Immunology, National Institute of Neuroscience, NCNP, 4-1-1 Ogawahigashi, Kodaira, Tokyo 187-8502, Japan*
[b]*Department of Rheumatology, Juntendo University School of Medicine, 2-1-1 Hongo, Bunkyo-ku, Tokyo 113, Japan*

Received 27 April 2004; revised 15 September 2004; accepted 29 September 2004

Abstract

Non-obese diabetic (NOD) mice develop diabetes mediated by pathogenic T-helper type 1 (Th1) cells. Vα14 Natural killer (NKT) cells are a unique lymphocyte subtype implicated in the regulation of autoimmunity and a good source of protective Th2 cytokines. We recently developed a Th2-skewing NKT cell ligand, OCH. OCH, a sphingosine truncated derivative of α-galactosylceramide (α-GC), stimulates NKT cells to selectively produce Th2 cytokines. Here we show that OCH prevented the development of diabetes and insulitis in NOD mice. The suppression of insulitis by OCH was more profound compared to α-GC. Infiltration of T cells, B cells and macrophages into islets is inhibited in OCH-treated NOD mice. OCH-mediated suppression of diabetes is associated with Th2 bias of anti-islet antigen response and increased IL-10 producing cells among islet-infiltrating leukocytes. Considering the non-polymorphic and well conserved features of the CD1d molecule in mice and humans, these findings not only support the proposed role of NKT cells in the regulation of self-tolerance but also highlight the potential use of OCH for therapeutic intervention in type I diabetes.

Keywords: NKT cells; Autoimmune disease; Type I diabetes; NOD mice; Glycolipid

1. Introduction

Non-obese diabetic (NOD) mice develop spontaneous autoimmune (type I) diabetes (T1D) very similar to the human disease. In female mice, insulitis usually begins at 3 to 5 weeks of age, eventually leading to β-cell destruction and overt diabetes by 4 to 6 months of age. Autoimmune destruction of β-cells is preceded by infiltration of pancreatic islets by macrophages, B cells and T cells. The capacity to transfer disease by islet specific T cells purified from diabetic NOD mice or T cell clones demonstrates the key role of T cells in the pathogenesis of diabetes. Th1 type CD4 cells, which preferentially secrete IFN-γ and TNF-α and CD8 T cells, have been implicated in the development of diabetes in NOD mice [1,2]. In parallel with these effector T cells, regulatory cells including $CD4^+CD25^+$ T cells have been suggested to inhibit the development of diabetes. Although the mechanisms of suppressive effect of these regulatory T cells are not fully understood, it is believed that an imbalance between autoreactive effector T cells and regulatory T cells may trigger the development of destructive insulitis and T1D [3]. Previous studies indicate that the β-cell-destructive immune response in NOD mice is biased toward Th1 and treatment with Th2 cytokines such as IL-4 or IL-10 have been shown to prevent the onset of spontaneous diabetes [4–8].

* Corresponding author. Tel.: +81 42 341 2711; fax: +81 42 346 1753.
E-mail address: miyake@ncnp.go.jp (S. Miyake).

0896-8411/$ - see front matter © 2004 Elsevier Ltd. All rights reserved.
doi:10.1016/j.jaut.2004.09.008

Natural killer T (NKT) cells are a unique subset of T cells that coexpress receptors of the NK lineage and α/β T cell receptor (TCR) [9–11]. NKT cells express an invariant TCRα chain (encoded by a Vα14-Jα281 rearrangement in mice and a homologous Vα24-Jα15 rearrangement in humans). Unlike conventional T cells that recognize peptides in association with MHC, NKT cells recognize glycolipid antigens such as α-galactosylceramide (α-GC) bound by the non-polymorphic MHC class I-like protein CD1d [12]. One striking feature of NKT cells is their capacity to secrete large amounts of cytokines including IL-4 and IFN-γ in response to TCR ligation. Although the precise function of NKT cells remains to be elucidated, evidence indicates that NKT cells play critical roles in the regulation of autoimmune responses [13–15]. Abnormalities in the number and function of NKT cells have been observed in patients with autoimmune diseases as well as in a variety of mouse strains that are genetically predisposed for development of autoimmune diseases. The putative involvement of NKT cells in the control of islet β-cell reactive T cells in NOD mice was suggested by prevention of diabetes following infusion of NKT cell-enriched thymocyte preparations [16] and by over-expression of NKT cells in Vα14-Jα281 transgenic NOD mice [17]. Moreover, several recent studies have investigated the effect of treating NOD mice with α-GC [18–21]. When started at around 3 or 4 weeks of age, repeated injections at least once a week delayed the onset and reduced the incidence of diabetes by inducing Th2 bias of autoreactive T cells. We have recently developed a synthetic glycolipid ligand, OCH, which stimulates NKT cells to selectively produce IL-4. OCH is a synthetic glycolipid, sphingosine truncation analogue of α-GC [22]. Administration of OCH inhibited experimental autoimmune encephalomyelitis (EAE) and collagen-induced arthritis (CIA) by inducing Th2 bias of autoreactive T cells [22,23]. These findings led us to examine the effect of OCH on the development of diabetes in NOD mice.

In the present study, we show that OCH can inhibit the development of insulitis and diabetes in NOD mice by inducing a Th2 bias of autoreactive T cells. These results imply that targeting NKT cells with OCH could be an attractive means for intervention in T1D.

2. Materials and methods

2.1. Mice

C57BL/6(B6) mice were purchased from CLEA Laboratory Animal Corp. (Tokyo, Japan). NOD/Shi mice were obtained from CLEA Japan (Tokyo, Japan). The animals were kept under specific pathogen-free conditions. We followed the guidelines for the use and care of laboratory animals of National Institute of Neuroscience, NCNP.

2.2. In vitro responses of NKT cells to α-GC or OCH

Splenocytes of naïve B6 mice were cultured with α-GC or OCH in RPM I1640 medium supplemented with 5×10^{-5} M 2-ME, 2 mM L-glutamine, 100 U/mg/ml penicillin/streptomycin, and 1% syngenic mouse serum for 72 h. Incorporation of [^{3}H]-thymidine (1 μCi/well) for the final 16 h of the culture was determined with a β-1205 counter (Pharmacia, Uppsala, Sweden). The levels of IL-4, IL-10 and IFN-γ in culture supernatant were measured by a standard sandwich ELISA, using purified and biotinylated antibody pairs and standards from BD PharMingen (San Jose, CA).

2.3. In vivo responses of NKT cells to α-GC or OCH

NOD mice were injected with 100 μg/kg of OCH or α-GC intraperitoneally and serum were collected after 2 h, 6 h and 24 h after injection. Serum levels of IL-4, IL-10 and IFN-γ were measured by ELISA.

2.4. Assessment of diabetes and evaluation of insulitis

Diabetes was assessed by monitoring glucose levels every week in the blood using GLU-W (Fujifilm, Kanagawa, Japan). Mice with two consecutive positive blood glucose measurements greater than 250 mg/dl were considered diabetic. For histological evaluation of insulitis, mice were killed and pancreata were removed and fixed with 4% paraformaldehyde. Sections were stained with hematoxylin and eosin (HE). Multiple HE stained pancreatic sections were scored. Insulitis was graded as follows: grade 0, no inflammation; grade 1, peri-insulitis but no intra-insulitis; grade 2, mild intra-insulitis (cell infiltration in the area less than 25% of an islet); grade 3, moderate intra-insulitis (cell infiltration in the area more than 25% but less than 50% of an islet); and grade 4, severe intra-insulitis (cell infiltration in the area more than 50% of an islet).

2.5. Immunohistochemistry

Immunohistochemistry was performed on 15-mm-thick adjacent serial sections according to the avidin–biotin–peroxidase complex (ABC) method using ABC Elite (Vector) and 3,3′-diaminobenzidine tetrahydrochloride (DAB) as chromogen. Primary antibodies were used as follows; mouse CD4 (RM4-5, BD PharMingen), mouse CD8a (53-6.7, BD PharMingen), mouse B220 (RA3-6B2, BD PharMingen), mouse F4/80 antigen (A3-1, Serotec), mouse CD45 (sc-1121, Santa Cruz

Biotechnology Inc.), mouse interleukin-4 (11B11, ATCC), mouse interleukin-10 (JES-2A5), and mouse interferon-γ (XMG1.2, BD PharMingen). The biotinylated goat anti-mouse antibody or the biotinylated rabbit anti-goat antibody (Vector, Burlingame, CA, USA) was used as a secondary antibody. Cell infiltration was graded as follows: no infiltration, peri-infiltration, cell infiltration in peri-islet area but no intra-islet; mild infiltration, cell infiltration in less than 50% of the area of an islet; severe infiltration, cell infiltration in more than 50% of the area of an islet. For the quantification of cytokine staining, more than 100 CD45 positive cells per mice (five animals in each group) were evaluated for the IL-4 or IL-10 staining.

2.6. In vivo glycolipids treatment

α-GC and OCH were synthesized as described previously [24]. Synthetic glycolipids were used to treat NOD mice. Starting from 5 weeks of age, mice were injected intraperitoneally twice per week with either OCH or α-GC at a dose of 100 μg/kg. The control mice were injected with vehicle alone (10% DMSO in PBS).

2.7. Measurement of autoantigen specific IgG1 and IgG2a

Anti-glutamic acid decarboxylase (GAD) was measured by ELISA as described previously [19,25]. GAD (Sigma) (1 mg/ml) was coated onto ELISA plates (Sumitomo Bakelite, Co., Ltd, Tokyo, Japan) at 4 °C overnight. After blocking with 1% bovine serum albumin in PBS, serially diluted serum samples were added onto GAD-coated wells. For detection of anti-GAD antibodies, the plates were incubated with biotin-labeled anti-IgG1 and anti-IgG2a (Southern Biotechnology Associates, Inc., Brimingham, AL) or anti-IgG antibody (CN/Cappel, Aurora, OH) for 1 h and then incubated with streptavidin-peroxidase. After adding a substrate, the reaction was evaluated and antibody titers were calculated on the basis of dilution/absorbance curves. To control the experiments, dilutions of anti-GAD-positive serum from diabetic NOD mice were used as the control samples. Based on the standard values of the control samples, the relative value for each test sample was displayed.

3. Results

3.1. OCH induces selective production of Th2 cytokines in NOD mice

NOD mice have been reported to exhibit the defect in the number and the function of NKT cells [26]. We first examined whether OCH stimulates proliferation and selective IL-4 production in NOD mice. Spleen cells from NOD mice proliferated in response to in vitro stimulation with OCH and produced significant amounts of IL-4 and IL-10, although OCH was less active in inducing cell proliferation and the cytokine production compared with α-GC (Fig. 1A). In contrast, IFN-γ was barely detectable in response to OCH stimulation, whereas α-GC induces massive IFN-γ production (Fig. 1A). We next examined whether OCH treatment in vivo also induces the selective Th2 cytokines. We injected OCH or α-GC intraperitoneally in NOD mice and measured the serum level of IL-4, IL-10 and IFN-γ by ELISA. Consistent with in vitro data, OCH injection induced a rise in IL-4 and IL-10 (Fig. 1B, left and right panels) along with much less increase in the levels of IFN-γ (Fig. 1B, middle panel). In contrast, injection of α-GC induced the production of IL-4, IL-10 and IFN-γ. These results suggest that OCH preferentially induces Th2 cytokines in NOD mice similar to B6 mice.

3.2. OCH treatment prevents diabetes and insulitis in NOD mice

IL-4 and IL-10 have been reported as important protective cytokines for diabetes in NOD mice [4–8,16]. Thus, we tested whether multiple injections of OCH to NOD mice can modulate the development of diabetes. As shown in Fig. 2A, treatment of OCH starting at 5 weeks of age significantly delayed the onset and reduced the incidence of diabetes from 75% to 27% in female NOD mice at 30 weeks of age. α-GC inhibited the development of diabetes as well as previously described [18–21].

Next we examined HE-stained sections from pancreata of mice treated with either glycolipid ligands or vehicle twice per week from the age of 5 weeks. As shown in Fig. 2B, significantly greater percentages of islets were free of insulitis from OCH-treated mice than those from the control mice. Fifty percent of islets were free of infiltrating cells in OCH-treated mice, at which time less than 20% of islets were from vehicle-treated mice. The percentage of islets affected by severe insulitis (grade 4) was significantly lower ($p = 0.023$, Dunnett's multiple comparison tests) and the frequency of intact islet (grade 0) was significantly higher ($p = 0.0038$, Dunnett's multiple comparison tests) in OCH-treated mice than in α-GC treated mice. The mean score of insulitis of α-GC- or OCH-treated mice was significantly lower than vehicle-treated mice. Typical histological appearance was shown in Fig. 2C. These results indicate that the inhibitory effect of insulitis by OCH is stronger than α-GC even though OCH was about less active in inducing NKT cell proliferation (Fig. 1A). We further examined whether a particular subset of cells are preferentially affected by OCH treatment at the age of

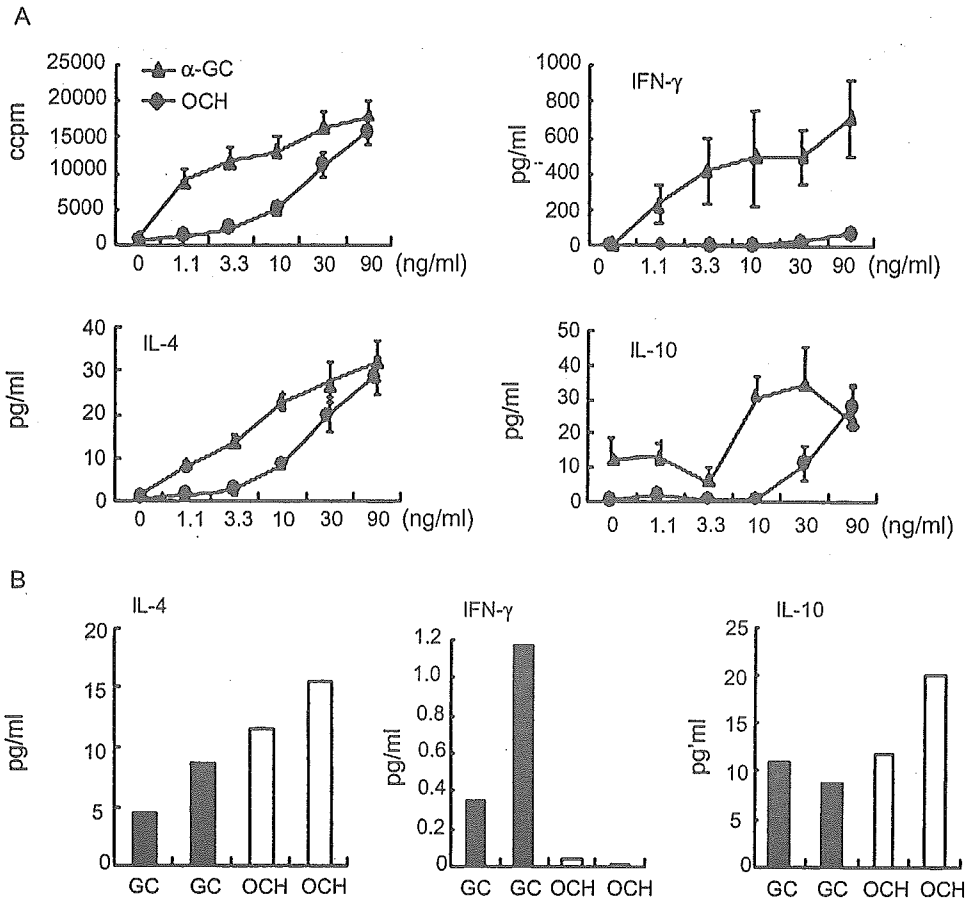

Fig. 1. Effects of OCH on cytokine production in NOD mice in vitro and in vivo. (A) Spleen cells were stimulated with various concentrations of glycolipid for 72 h. Incorporation of [^{3}H]-thymidine (1 μCi/well) for the final 16 h of the culture was examined (left top) and IFN-γ (right top), IL-4 (left bottom) or IL-10 (right bottom) contents in the supernatants were measured by ELISA. (B) Serum levels of IL-4, IFN-γ, IL-10 in NOD mice after intraperitoneal injection of OCH or α-GC were measured by ELISA. Data represent the individual mice and the peak level of each cytokine (2 h for IL-4, 24 h for IFN-γ and 6 h for IL-10) was displayed. Black bar: α-GC treated mice; white bar: OCH-treated mice.

16 weeks (Fig. 3). Massive infiltration of CD4 T cells, CD8 T cells, B cells into islets was observed in vehicle-treated NOD mice. Macrophages were also observed in vehicle-treated NOD mice. In contrast, OCH treatment inhibited infiltration of both T cells and B cells, and macrophages were barely detectable in OCH-treated mice. These results indicated that administration of OCH inhibited the development of diabetes and insulitis in NOD mice and the suppressive effect of insulitis is stronger than α-GC.

3.3. Administration of OCH promotes a Th2 response against autoantigens

To evaluate effects on immune responses against autoantigen, we measured GAD-specific IgG1 and IgG2a in the serum at the age of 24 weeks (Fig. 4, left and middle panels). The level of IgG2a was reduced both in OCH- and α-GC-treated mice compared to vehicle-treated mice. IgG1/IgG2a ratio significantly increases in OCH-treated mice. In α-GC-treated mice, IgG1/IgG2a ratio also tended to increase, even though the difference did not reach statistical significance. These results suggest that anti-GAD response in OCH-treated NOD mice shifted to Th2 response, and Th2 bias of autoantigen was more evident in OCH-treated mice compared to α-GC-treated mice.

3.4. OCH treatment increased IL-10 producing cells among islet-infiltrated leukocytes in NOD mice

Since anti-GAD response shifted to Th2 in OCH-treated mice, we next examined the numbers of IL-4 or IL-10 producing cells among the infiltrating leukocytes. IL-10 producing cells among CD45 positive leukocytes were significantly increased in OCH-treated mice compared to vehicle-treated NOD mice (Fig. 5). IL-4 producing cells were not significantly increased in OCH-treated mice. The frequency of either IL-4- or IL-10-producing cells among leukocytes in α-GC-treated mice were not significantly different from vehicle-treated mice. These results suggest that OCH-mediated

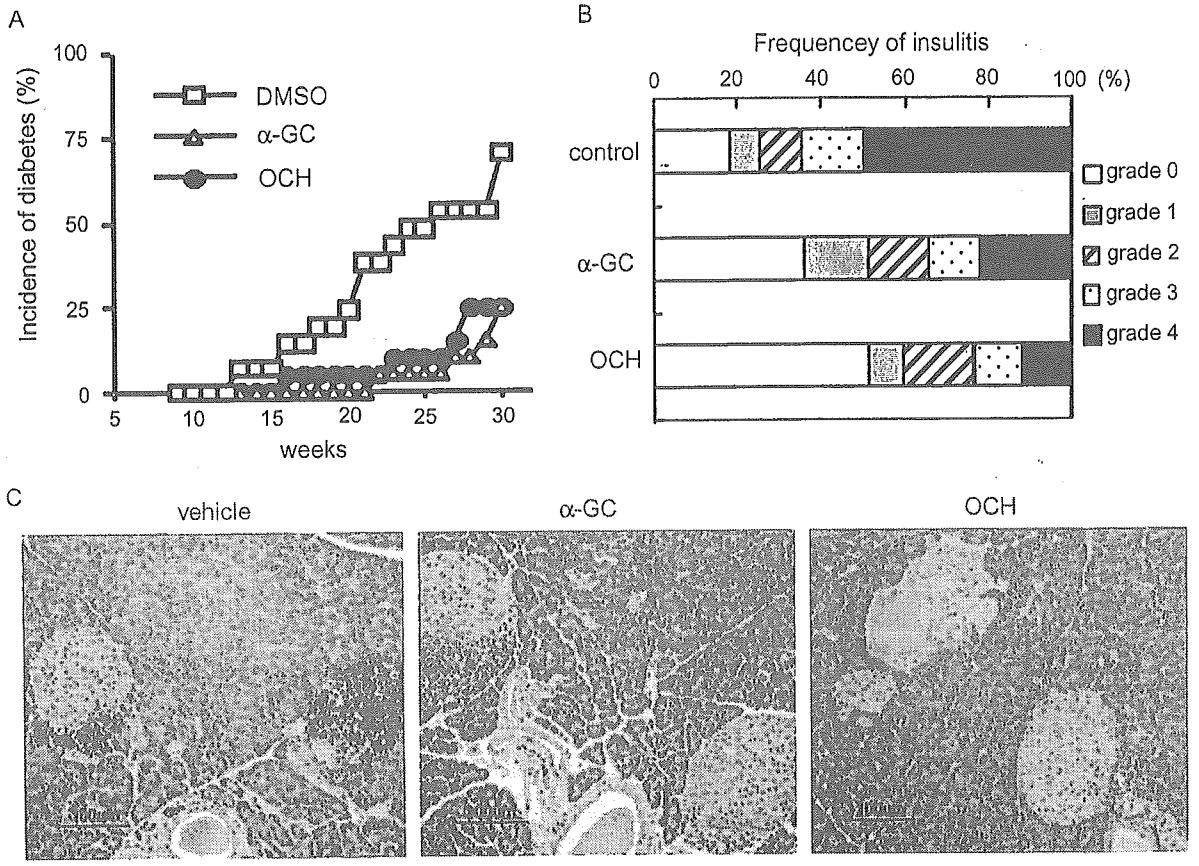

Fig. 2. Prevention of diabetes and insulitis in NOD mice by OCH treatment. (A) The effect of OCH on the incidence of diabetes. Female NOD mice were injected with OCH, α-GC or vehicle twice per week starting at 5 weeks of age ($n = 20$ per group). Diabetes was monitored by measurements of blood glucose levels. (B) Female NOD mice were treated with OCH, α-GC or vehicle twice per week starting at 5 weeks of age. Pancreata were microscopically evaluated for the degree of insulitis at 16 weeks of age. Data shown represent the mean of six animals in each group and more than 20 islets per mice were scored for grading as described in Section 2. The mean score of insulitis of vehicle-, α-GC-, or OCH-treated mice was 1.56, 1.24, 2.7 ($p < 0.001$; vehicle vs α-GC, $p < 0.001$; vehicle vs OCH, $p < 0.0081$; α-GC vs OCH). (C) Representative histological appearance of hematoxylin and eosin-stained islets from non-diabetic female NOD mice treated with vehicle, α-GC, or OCH used in the experiments shown in (B).

inhibition of insulitis is associated with increase of IL-10 producing cells.

4. Discussion

In this study, we found that OCH treatment prevented spontaneous autoimmune diabetes in NOD mice, a model of human type I diabetes, by inducing Th2 bias. OCH treatment strongly inhibited insulitis in NOD mice. The proportion of IL-10 producing cells among infiltrated leukocytes was increased in OCH-treated mice. Although the correlation between a defect in NKT cells and the susceptibility of diabetes in NOD mice is still debated [13–15], the putative involvement of NKT cells in the control of islet β-cell reactive T cells in NOD mice was suggested by the prevention of diabetes following an infusion of NKT cell-enriched thymocytes [16], and by the increase of NKT cells in Vα14-Jα281 transgenic NOD mice [17]. In these mice, protection from diabetes by NKT cells is associated with the induction of a Th2 response to islet autoantigens. Furthermore, α-GC treatment has been demonstrated to delay the onset and reduce the incidence of diabetes in NOD mice [18–21]. And the mechanism of protection has been reported to be associated with Th2 shift of autoantigen response, which is similar to that observed by increasing the number of NKT cells in NOD mice. The mechanism of OCH-mediated inhibition of insulitis was also associated with Th2 polarization of the autoantigen response and increase of IL-10 producing cells. The stronger suppression of insulitis by OCH treatment than α-GC treatment may not be surprising because α-GC stimulates NKT cells to produce IFN-γ as well as Th2 cytokines. IFN-γ enhances the expression of major histocompatibility complex class I and II molecules as well as several other proteins involved in antigen processing and presentation, and supports the homing of activated T cells into islets in NOD mice [27–29].

Stimulation of NKT cells by injection of OCH inhibited EAE and CIA [22,23]. On the other hand,

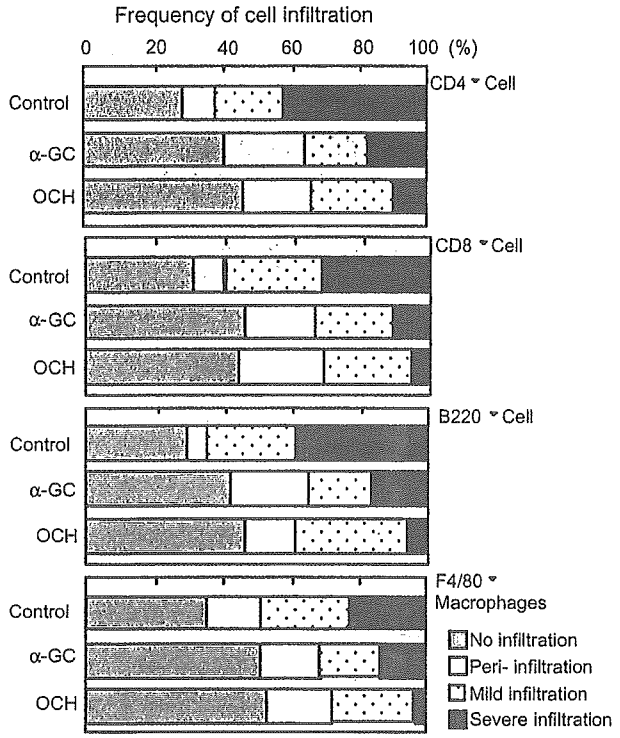

Fig. 3. Immunohistochemical analysis of cell composition of infiltrated cells into islets in NOD mice treated with OCH. Female NOD mice were treated with OCH, α-GC or vehicle twice per week starting at 5 weeks of age. At 16 weeks of age, pancreata were microscopically evaluated for the degree of infiltrated cells positive for CD4, CD8, B220 or F4/80 antigen as described in Section 2. Data shown represent the mean of six animals in each group and more than 20 islets per animal.

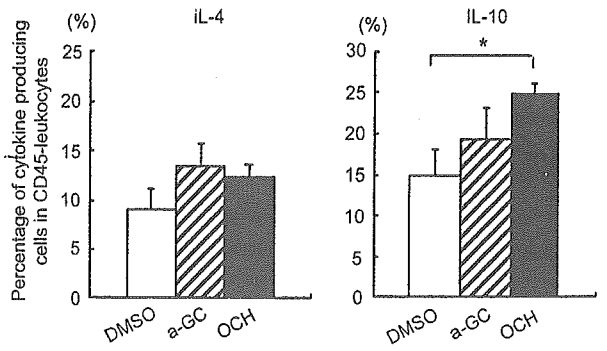

Fig. 5. Immunohistochemical analysis of IL-4 or IL-10 producing cells infiltrated into islets in NOD mice treated with OCH. Female NOD mice were injected with OCH, α-GC or vehicle twice per week starting at 5 weeks of age. Immunohistochemical examination was performed at 16 weeks of age. Data shown represent the mean of six animals in each group and more than 100 $CD45^+$ leukocytes per mice were evaluated. IL-4 positive or IL-10 positive cells were expressed as percentage of $CD45^+$ total leukocytes. $^*p = 0.017$ vs control, by Dunnett's multiple comparison tests.

α-GC ameliorates or exacerbates EAE, depending on the strain of mouse and stage of disease tested [30–32] and to have only a marginal effect on CIA [23], probably because α-GC induces both Th1 and Th2 cytokines whereas OCH predominantly elicits a Th2 response. In this situation, treatment with OCH might be preferable to α-GC for Th1-mediated diseases. Although the insulitis was severe in α-GC-treated mice compared to OCH-treated mice, we confirmed that multiple injection of α-GC inhibited diabetes in NOD mice as well as OCH as previously reported [18–21]. There might be several reasons to explain that the effect of OCH was not different in the inhibition of overt diabetes. For example, it has been documented that no modification of the diabetes incidence occurs in both IFN-γ knockout and IFN-γ receptor knockout mice, as compared with littermate controls. Therefore α-GC induced IFN-γ has less effect to mask the protective effect of Th2 cytokines in NOD mice, which is different to other models such as EAE or CIA. The other possibility to explain that OCH and α-GC showed similar effect on the development of overt diabetes is that diabetes in NOD mice develops spontaneously and multiple injection of α-GC or OCH were continued for several months, which are different from other inducible autoimmune models. The adjuvant used for the induction of other models such as EAE and CIA might have some effect on the cytokine production by NKT cells. Considering that the bacterial infection has been shown to induce predominantly Th1 cytokines from NKT cells [33], injection of α-GC at the same time the injection of CFA including mycobacterium extract could enhance Th1 cytokine production from NKT cells

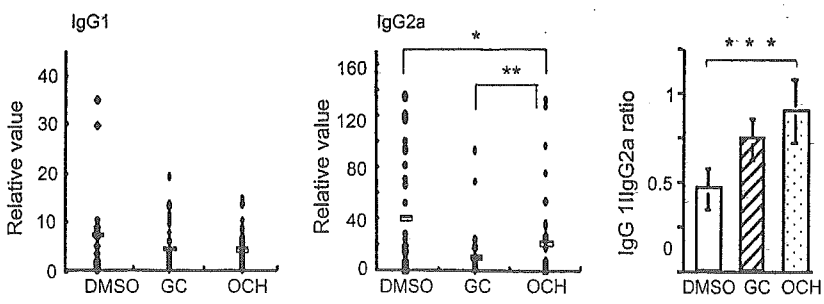

Fig. 4. GAD-specific antibody isotype levels in mice treated with OCH. Individual serum samples obtained from mice shown in Fig. 2 at 24 weeks were analyzed as in Section 2. IgG1:IgG2a ratios in OCH-, α-GC-, vehicle-treated mice are shown. Values are the mean and SEM ($n = 20$). $^*p = 0.0327$, $^{***}p = 0.0147$, OCH vs control, $^{**}p = 0.0002$, α-GC vs control by Mann–Whitney U test.

enough for the mask of the inhibitory effect of Th2 cytokines. In contrast, in NOD mice which spontaneously develop diabetes, Th1 cytokine production from NKT cells for the initial treatment might not be so harmful because NKT cells have been reported to have the tendency to predominantly produce Th2 cytokines after repeated injections [34] since the glycolipid treatment was continued for several months.

It is still controversial whether the defects in NKT cells are causal for autoimmune disease or occur as a secondary consequence of the autoimmune process [13–15]. However, given the efficacy of glycolipid ligands such as OCH in the prevention of the development of diabetes in NOD mice, in addition to the suppression of EAE and CIA, stimulation of NKT cells with glycolipid seems to be an attractive strategy for the treatment of autoimmune diseases such as type I diabetes. The evolutionary conservation and the homogeneous ligand specificity of NKT cells allow us to apply a glycolipid ligand like OCH for the treatment of human disease without considering species barrier or genetic heterogeneity of humans.

Acknowledgements

This work was supported by the Pharmaceuticals and Medical Devices Agency (PMDA), Grant-in-Aid for Scientific Research (B) 14370169 from Japan Society for the Promotion of Science, Uehara Memorial Foundation, Kato Memorial Bioscience Foundation and Kanae Foundation for Life & Socio-Medical Science.

References

[1] Bach JF. Insulin-dependent diabetic mellitus as an autoimmune disease. Endocr Rev 1994;15:516–42.
[2] Delovitch TL, Singh B. The nonobese diabetic mouse as a model of autoimmune diabetes: immune dysregulation gets the NOD. Immunity 1997;7:727–38.
[3] Bach JF, Chatenoud L. Tolerance to islet autoantigens in type 1 diabetes. Ann Rev Immunol 2001;19:131–61.
[4] Rapoprt MJ, Jaramillo A, Zipris D, Lazarus AH, Serreze DV, Leiter EH, et al. Interleukin 4 reverses T cell proliferative unresponsiveness and prevents the onset of diabetes in nonobese diabetic mice. J Exp Med 1993;178:87–99.
[5] Pennline KJ, Roque-Gaffney E, Monahan M. Recombinant human IL-10 prevents the onset of diabetes in the nonobese diabetic mouse. Clin Immunol Immunopathol 1994;71:169–75.
[6] Zheng XX, Steele AW, Hancock WW, Stevens C, Nickerson PW, Roy-Chaudhury P, et al. A noncytolytic IL-10/Fc fusion protein prevents diabetes, blocks autoimmunity, and promotes suppressor phenomena in NOD mice. J Immunol 1997;158:4507–13.
[7] Goudy K, Song S, Wasserfall C, Zhang YC, Kapturczak M, Muir A, et al. Adeno-associated virus vector-mediated IL-10 gene delivery prevents type 1 diabetes in NOD mice. Proc Natl Acad Sci U S A 2001;98:13913–8.
[8] Yang Z, Chen M, Wu R, Fialkow LB, Bromberg JS, McDuffie M, et al. Suppression of autoimmune diabetes by viral IL-10 gene transfer. J Immunol 2002;168:6479–85.
[9] Bendelac A, Rivera MN, Park SH, Roark JH. Mouse CD1-specific NK1 T cells: development, specificity, and function. Annu Rev Immunol 1997;15:535–62.
[10] Porcelli SA, Modlin RL. The CD1 system: antigen-presenting molecules for T cell recognition of lipids and glycolipids. Annu Rev Immunol 1999;17:297–329.
[11] Kronenberg M, Gapin L. The unconventional lifestyle of NKT cells. Nat Rev Immunol 2002;2:557–68.
[12] Kawano T, Cui J, Koezuka Y, Toura I, Kaneko Y, Motoki K, et al. CD1-restricted and TCR-mediated activation of Vα14 NKT cells by glycosylceramides. Science 1997;278:1626–9.
[13] Hammond KJL, Godfrey DI. NKT cells: potential targets for autoimmune disease therapy? Tissue Antigens 2002;59:353–63.
[14] Hammond KJL, Kronenberg M. Natural killer T cells: natural or natural regulators of autoimmunity? Curr Opin Immunol 2003; 15:683–9.
[15] Wilson SB, Delovitch TL. Janus-like role of regulatory iNKT cells in autoimmune disease and tumour immunity. Nat Rev Immunol 2003;3:211–22.
[16] Hammond KJL, Poulton LD, Palmisano LJ, Silveria PA, Godfrey DJ, Baxter AG. α/β-T cell receptor (TCR)+CD4-CD8-(NKT) thymocytes prevent insulin-dependent diabetes mellitus in nonobese diabetic (NOD)/Lt mice by the influence of interleukin (IL)-4 and/or IL-10. J Exp Med 1998;187:1047–1056.
[17] Lehuen A, Lantz O, Beaudoin L, Laloux V, Carnaud C, Bendelac A, et al. Overexpression of natural killer T cells protects Vα14-Jα281 transgenic nonobese diabetic mice against diabetes. J Exp Med 1998;188:1831–9.
[18] Hong SH, Wilson MT, Serizawa I, Wu L, Singh N, Naidenko OV, et al. The natural killer T-cell ligand α-galactosylceramide prevents autoimmune diabetes in non-obese diabetic mice. Nat Med 2001;7:1052–6.
[19] Sharif S, Arreaza GA, Zucker P, Mi Q-S, Sondhi J, Naidenko OV, et al. Activation of natural killer T cells by α-galactosylceramide treatment prevents the onset and recurrence of autoimmune type 1 diabetes. Nat Med 2001;7:1057–62.
[20] Wang B, Geng YB, Wang CR. CD1-restricted NK T cells protect nonobese diabetic mice from developing diabetes. J Exp Med 2001;194:313–9.
[21] Naumov YN, Bahjat KS, Gausling R, Abraham R, Exley MA, Koezuka Y, et al. Activation of CD1d-restricted T cells protects NOD mice from developing diabetes by regulating dendritic cell subsets. Proc Natl Acad Sci U S A 2001;98: 13838–43.
[22] Miyamoto K, Miyake S, Yamamura T. A synthetic glycolipid prevents autoimmune encephalomyelitis by inducing Th2 bias of natural killer T cells. Nature 2001;413:531–4.
[23] Chiba A, Oki S, Miyamoto K, Hashimoto H, Yamamura T, Miyake S. Suppression of collagen-induced arthritis by natural killer T cell activation with OCH, a sphingosine-truncated analog of α-galactosylceramide. Arthritis Rheum 2004;50:305–13.
[24] Oki S, Chiba A, Yamamura T, Miyake S. The clinical implication and molecular mechanism of preferential IL-4 production by modified glycolipid-stimulated NKT cells. J Clin Invest 2004;113: 1631–40.
[25] Laloux V, Beaudoin L, Jeske D, Carnaud C, Lehuen A. NKT cell-induced protection against diabetes in Vα14Jα281 transgenic nonobese diabetic mice is associated with a Th2 shift circumscribed regionally to the islets and functionally to islet autoantigen. J Immunol 2001;166:3749–56.
[26] Gombert JM, Herbelin A, Tancrede-Bohin E, Dy M, Carnaud C, Bach J-F. Early quantitative and functional deficiency of NK1$^+$-like thymocytes in the NOD mouse. Eur J Immunol 1996;26: 2989–98.
[27] Wang B, Andre I, Gonzalez A, Katz JD, Aguet M, Benoist C, et al. Interferon-γ impacts at multiple points during the

progression of autoimmune diabetes. Proc Natl Acad Sci U S A 1997;94:13844–9.
[28] Savinov AY, Wong FS, Chervonsky AV. IFN-γ affects homing of diabetogenic T cells. J Immunol 2001;167:6637–43.
[29] Hill NJ, Gunst KV, Sarvetnick N. Th1 and Th2 pancreatic inflammation differentially affects homing of islet-reactive CD4 cells in nonobese diabetic mice. J Immunol 2003;170:1649–58.
[30] Jahng AW, Maricic I, Pedersen B, Burdin N, Naidenko O. Activation of natural killer T cells potentiates or prevents experimental autoimmune encephalomyelitis. J Exp Med 2001; 194:1789–99.
[31] Singh AK, Wilson MT, Hong S, Oliveres-Villagomez D, Du C, Stanic AK, et al. Natural killer T cell activation protects mice against experimental autoimmune encephalomyelitis. J Exp Med 2001;194:1801–11.
[32] Furlan R, Bergami A, Cantarella D, Brambilla E, Taniguchi M, Dellabona P, et al. Activation of invariant NKT cells αGalCer administration protects mice from MOG_{35-55}-induced EAE: critical roles for administration route and IFN-γ. Eur J Immunol 2003;33:1830–8.
[33] Brigl M, Bry L, Kent SC, Gumperz JE, Brenner MB. Mechanism of CD1d-restricted natural killer T cell activation during microbial infection. Nat Immunol 2003;12:1230–7.
[34] Burdin N, Brossay L, Kronenberg M. Immunization with α-galactosylceramide polarizes CD1-reactive NKT cells towards Th2 cytokine synthesis. Eur J Immunol 1999;29:2014–25.

Journal of Neuroscience Research 78:141–150 (2004)

Glycosphingolipid Composition of Primary Cultured Human Brain Microvascular Endothelial Cells

Takashi Kanda,[1]* Toshio Ariga,[2] Hisako Kubodera,[1] Hong Lian Jin,[1] Kiyoshi Owada,[1] Takeshi Kasama,[3] Masanaga Yamawaki,[1] and Hidehiro Mizusawa[1]

[1]Department of Neurology and Neurological Science, Tokyo Medical and Dental University Graduate School, Tokyo, Japan

[2]Drug Development Technology, Eisai Co. Ltd., Tokyo, Japan

[3]Instrumental Analysis Research Center of Life Science, Tokyo Medical and Dental University Graduate School, Tokyo, Japan

Glycosphingolipid (GSL) antigens have been considered to be involved in the pathogenesis of autoimmune neurologic disorders including multiple sclerosis. To establish the GSL pattern specific for endothelial cells forming blood–brain barrier (BBB), we established a method to yield sufficient quantities of highly purified human brain microvascular endothelial cells (HBMECs) and compared their GSL composition to that of human umbilical cord vein endothelial cells (HUVECs), as the representative of endothelial cells not forming BBB. The major gangliosides were GM3 and sialyl paragloboside (LM1), and the major neutral GSLs were lactosylceramide (LacCer), globotriaosylceramide (Gb3), and globoside (Gb4). Trace amounts of GM1, GD1a, GD1b, GT1b, and sulfoglucuronosyl paragloboside (SGPG) could be detected by the high performance thin layer chromatography-overlay method. SGPG was detected only at a nonconfluent state in an amount almost 1/30 that of in nonconfluent HUVECs. Conversely, GM3 and LM1 increased significantly after confluency. The amount of Gb3 in HBMECs was almost as twice that in HUVECs. The significance of these differences in GSL content between HBMECs and HUVECs and between confluent and nonconfluent states is obscure. It might be related, however, to the defense mechanism at the BBB and to the susceptibility of the central nervous system in some disorders that target cell surface GSL, such as hemolytic uremic syndrome.

Key words: glycosphingolipid; sulfoglucuronosyl paragloboside; blood–brain barrier; human brain microvascular endothelial cell

Vascular endothelial cells (ECs) are highly versatile cells and are involved structurally as well as metabolically in various barrier functions. The characteristic features of ECs include the presence of nonthrombogenic luminal surface, expression of von Willebrand factor, prostacycline, and endothelin, and formation of a highly selective barrier to the passage of plasma constituents into the tissue parenchyma. ECs possess many structural and functional characteristics, exhibiting a wide diversity depending on the nature of the vascular bed; this property is very important for their specialized function in individual tissue and organ function (Jaffe, 1987; Kanda et al., 1994). ECs of brain microvascular origin (BMECs) are highly specialized cells believed to make up the structural basis of the blood–brain barrier (BBB). Because BMECs are the only cell groups in the nervous system that are exposed continuously to blood constituents, the information via surface receptors on BMECs are considered very important for regulation of BBB function and subsequently for homeostasis of various cations, nutrients, and growth factors in the central nervous system (CNS).

Glycosphingolipids (GSLs) are located primarily, if not exclusively, on the outer leaflet of the plasma mem-

Abbreviations: BBB, blood–brain barrier; BMEC, brain microvascular endothelial cell; BNB, blood–nerve barrier; CNS, central nervous system; DiI-Ac-LDL, 1, 1′-dioctacecyl-3,3,3′,3, tetramethyl indocarbocyanine perchlorate acetylated low-density lipoprotein; DM, Dissecting medium; EC, endothelial cell; Gb3, globotriaosylceramide; Gb4, globoside; GSL, glycosphingolipid; HBMEC, human brain microvascular endothelial cell; HPTLC, high-performance thin-layer chromatography; HUS, hemolytic uremic syndrome; HUVEC, human umbilical cord vein endothelial cell; LM1, sialyl paragloboside; LacCer, lactosylceramide; *mdr1*, multidrug resistance-1 gene; PBS, phosphate buffered-saline; PnMEC, microvascular endothelial cell of endoneurial tissue origin; PNS, peripheral nervous system; SGPG, sulfoglucuronosyl paragloboside; SIMS, matrix-assisted secondary ion mass spectrometry.

Contract grant sponsor: Ministry of Education, Science, and Culture of Japan.

*Correspondence to: Dr. Takashi Kanda, Department of Neurology and Neurological Science, Tokyo Medical and Dental University Graduate School, 1-5-45, Yushima, Bunkyo-ku, Tokyo 113-8519, Japan.
E-mail: t-kanda.nuro@tmd.ac.jp

Received 12 February 2004; Revised 25 May 2004; Accepted 1 June 2004

Published online 23 August 2004 in Wiley InterScience (www.interscience.wiley.com). DOI: 10.1002/jnr.20228

brane. GSLs, including gangliosides, have been implicated in various cellular functions such as cellular recognition and adhesion, communication, and modulation of immune responses (Kanda et al., 1995; Karlsson, 1995; Riboni et al., 1997). Knowledge about GSLs as surface antigens and receptors in BMECs is therefore crucial to understanding the pathogenesis of CNS disorders affecting the BBB. Because of the difficulty in primary culture and the maintenance of human BMECs (HBMECs), however, no data concerning the GSL composition in these cells has ever been published. Duvar et al. (2000) recently investigated the GSL composition of immortalized human cerebromicrovascular endothelial cells; however, because this endothelial cell line cannot exclude the influence of immortalization with SV40 T-antigen, GSL analysis of genuine primary cultured HBMECs has been awaited eagerly.

We recently developed a method to yield sufficient quantities of highly purified HBMECs for biochemical analysis, and we have determined the GSL composition of cultured HBMECs. The aim of this article is to establish the GSL pattern specific for the ECs forming BBB, compared to that of human umbilical cord vein endothelial cells (HUVECs) as the representative of ECs without BBB property.

MATERIALS AND METHODS

Culture Media for HBMECs

Dissecting medium (DM) contained Medium 199 (GIBCO BRL, Grand Island, NY) supplemented with 5% fetal bovine serum (FBS; BioWhittaker, Walkersville, MD), 20 mM sodium bicarbonate, 50 μg/ml heparin (Sigma, St. Louis, MO), 100 U/ml penicillin, 100 μg/ml streptomycin, 25 ng/ml amphotericin B (GIBCO BRL), and 20 mM *N*-(2-hydroxymethyl)-piperazine-*N'*-(2-ethanesulfonic acid) (HEPES; pH 7.2). HBMEC growth medium contained EBM-2 media (Sanko Jun-yaku, Tokyo, Japan) supplemented with 100 U/ml penicillin, 100 μg/ml streptomycin, and 25 ng/ml amphotericin B.

Isolation of HBMECs

HBMEC isolation was achieved using a modified method of Gordon et al. (1991), which was designed originally for rat capillary endothelial cells. Brain tissue was removed approximately 6 hr postmortem from a 65-year-old male who had suffered from lung cancer. The tissue was rinsed thrice with DM, and the pia mater and surface vessels were removed carefully using fine forceps. The cerebral cortex was then minced to 2–3-mm cubes, rinsed several times in DM, and homogenized using a Wheaton-Dounce Teflon homogenizer. The homogenate was dissociated further with 0.005% (wt/vol) dispase (grade 1; Roche Diagnostics, Mannheim, Germany) in DM at 37°C for 2 hr in a shaking water bath. After centrifugation (800 × *g*, 5 min) the pellet was suspended with a dextran solution (mol. wt. 70,000 Daltons; 15% wt/vol in DM; Sigma), and the whole suspension was centrifuged (4°C, 4,500 × *g* for 10 min, using a Beckman JS 13.1 swinging bucket rotor). The pellet was resuspended with the dextran solution, and centrifuged again. After two centrifugations, microvessels and some single cells including red blood cells were obtained in the pellet. Other contaminating fractions including myelin and brain parenchyma were floated. The pellet was recovered with DM and filtered through 130-μm nylon mesh (Nitex; Tetko Inc., Elmsford, NY) to remove large vessels. The filtrate was digested further using collagenase/dispase (0.035% wt/vol in 10 ml DM; Roche Diagnostics) at 37°C for 12 hr in a shaking water bath. The collagenase/dispase-treated microvessels were centrifuged (800 × *g*, 5 min), rinsed and suspended in 3.0 ml DM, and then filtered through double layers of 15-μm mesh to remove single cells, which were the largest sources of non-ECs, including astrocytes and pericytes. The unfiltered cell clusters were placed into dishes coated with type I collagen (Collaborative Biomedical Products, Bedford, MA). Cells were maintained at 37°C in an atmosphere of 5% CO_2 in a humidified incubator. The medium was changed three times a week.

After 24 hr, the first migrated ECs were observed from the edge of seeded cell clusters. When the EC colonies grew sufficiently large for cloning (usually more than 100 ECs), the medium was replaced by 0.25% pancreatin solution (GIBCO BRL). The colonies for cloning (free of contamination of non-ECs, including pericytes) were marked before pancreatin treatment. The colonies were detached as clumps of ECs, and the marked colonies were picked up using a Pasteur pipette and were dissociated briefly in 0.1% trypsin in Ca^{2+}, Mg^{2+}-free Hanks' solution for 3–4 min. Cells were seeded again on 35-mm Petri dishes coated with type I rat tail collagen. After 10–21 days, confluent HBMECs, almost free of contaminating non-ECs, were subcultured at a split ratio of 1:3–5.

Identification of HBMECs

HBMECs were identified by the following four criteria: an elongated cobblestone-like appearance; immunoreactivity to anti-von Willebrand factor antigen antibody; uptake of 1, 1'-dioctacecyl-3,3,3',3, tetramethyl indocarbocyanine perchlorate acetylated low-density lipoprotein (DiI-Ac-LDL; Biomedical Technologies Inc., Stoughton, MA) (Voyta et al., 1984); and the expression of the multidrug resistance-1 (*mdr1*) gene. To label with DiI-Ac-LDL, cells were incubated with 10 μg/ml of DiI-Ac-LDL at 37°C in HBMEC growth media for 4 hr. Cells were then washed once with probe-free media for 10 min, fixed with 4% paraformaldehyde for 30 min, and viewed under a fluorescent microscope. HBMECs incorporated the bright DiI-Ac-LDL particles into their cytoplasm. Only the lots of HBMECs with more than 98% of DiI-Ac-LDL-positive cells were used for further analysis. Contaminated cells other than endothelial cells were also evaluated using mouse anti-human antibodies against glial fibrillary acidic protein (GFAP; Sigma), α smooth muscle actin (BioGenex Laboratories, San Ramon, CA), and galactocerebroside (Sigma). Less than 1% of cells were immunoreactive with these antibodies. Expression of *mdr1* mRNA, one of the most reliable pieces of evidence of their BBB-forming endothelial cell origin, was confirmed using Takara Human 3K Chip v.3.0 (Takara, Tokyo, Japan). Absence of *mdr1* mRNA in HUVEC was also confirmed.

Isolation of Glycosphingolipids

Cultured HBMECs and HUVECs (purchased from Sanko Jun-Yaku), grown confluently or semiconfluently on 100-mm Petri dishes, were harvested by scraping from the Petri dishes,

TABLE I. Glycosphingolipid Composition of Cultured HBMECs and HUVECs†

Glycosphingolipid	HBMEC-C	HBMEC-NC	HUVEC-C	HUVEC-NC
Acidic				
GM3	1,226 ± 321	254 ± 110*	2,321 ± 166	1,226 ± 194
LM1	583 ± 103	178 ± 36**	879 ± 314	464 ± 81
GM1	7.1 ± 0.9	6.2 ± 1.6	8.5 ± 1.7	6.0 ± 0.5
GD1a	4.3 ± 0.6	3.7 ± 1.0	3.0 ± 0.9	2.6 ± 0.7
GD1b	Trace	Trace	Trace	Trace
GT1b	2.5 ± 1.0	2.7 ± 0.9	2.5 ± 0.5	1.8 ± 0.9
Neutral				
LacCer	295 ± 102	182 ± 88	368 ± 139	339 ± 54
Gb3	548 ± 131	612 ± 185	259 ± 66	269 ± 62
Gb4	1,852 ± 483	1,359 ± 383	1,195 ± 530	1,205 ± 304

†HBMEC-C, human brain microvascular endothelial cell, confluent state; HBMEC-NC, human brain microvascular endothelial cell, nonconfluent state; HUVEC-C, human umbilical cord vein endothelial cell, confluent state; HUVEC-NC, human umbilical cord vein endothelial cell, nonconfluent state. Values were expressed as ng ± SEM per mg protein; $n = 3$.
*$P < 0.05$ vs. HBMEC-C and $P < 0.01$ vs. HUVEC-C.
**$P < 0.01$ vs. HBMEC-C and $P < 0.05$ vs. HUVEC-C.

washed two times with PBS, pH 7.3, and homogenized in 0.5 ml of distilled water. *Nonconfluent* or *semiconfluent* culture denotes the condition where endothelial cell-free vacant space, more than 20% of total culture dish surface, is visible under inverted microscopy. These cells are expected to be still proliferating. *Confluent* culture denotes that the endothelial cells are tightly packed and no cell-free vacant space is recognizable under inverted microscopy. Cells within the fourth passage were used for GSL analysis. Protein concentrations were determined according to the method of Bradford (1976) using a Bio-Rad (Richmond, CA) protein assay kit and bovine serum albumin (BSA) as standard. Lipids were extracted with 5 ml of chloroform/methanol (1:1 by volume), and 5 ml of chloroform/methanol (1:2 by volume), successively. After evaporating the organic solvents under a nitrogen stream, lipids were dissolved in 0.5 ml chloroform/methanol/water (30:60:8 by volume; solvent A), and applied to a Sephadex LH-20 column (0.5 × 30 cm, 10-ml bed volume; Pharmacia Fine Chemicals), preequilibrated with solvent A. After the first 3 ml of effluent was discarded, the next 3 ml was collected as a GSL fraction (Yu et al., 1994). The GSL fraction was then applied to a DEAE-Sephadex A-25 column (2.0-ml bed volume; Pharmacia Fine Chemicals). The neutral GSL fraction was eluted with 20 ml of solvent A, and the acidic GSL fraction was eluted with 20 ml of chloroform/methanol/0.8 M sodium acetate (30:60:8 by volume; solvent B) (Yu et al., 1994). The acidic lipid fraction was evaporated to dryness and the residue was dissolved in 0.5 ml of solvent A, and then desalted by Sephadex LH-20 column as described above. The recovered gangliosides and sulfoglucuronosyl paragloboside (SGPG) were developed on a high-performance thin-layer chromatographic plate (HPTLC; Merck, Darmstadt, Germany) with the solvent system of chloroform/methanol/water containing 0.22% $CaCl_2 \cdot 2H_2O$ (55:45:10 by volume; solvent system I) and the bands were visualized by spraying the plate with resorcinol-HCl (Ando et al., 1978; Sekine et al., 1984).

The neutral GSL fraction was evaporated to dryness and the residue was subjected to mild alkaline treatment (0.5 ml of 0.4 N NaOH in methanol) at 40°C for 2 hr or room temperature overnight to remove phospholipids according to the method of Handa (1963). The reaction mixtures were applied to a Sephadex LH-20 column to remove salts as described above. Neutral GSL composition was examined by HPTLC. Before chromatography, the upper half of the plate was sprayed with 1% borate and the entire plate was activated for 30 min at 120°C to detect glucosyl ceramide and galactosyl ceramide. After application of the sample, the plate was developed with a solvent system of chloroform/methanol/water (65:35:5 by volume, solvent system II). Neutral GSLs were visualized by spraying with the orcinol-sulfuric acid reagent. The nomenclature of gangliosides follows the system of Svennerholm (1964).

Quantitation of GM3 (NeuAc), Sialyl Paragloboside (NeuAc-nLcOse$_4$), and Other Ganglio-*N*-Tetraosyl Gangliosides

The content of GM3 (NeuAc) and sialyl paragloboside (LM1) was determined by densitometric scanning of the chromatographic plate with comigration of authentic GM3 (NeuAc) and LM1, followed by visualizing with the resorcinol-HCl reagent (Ando et al., 1978). The structure of LM1 was confirmed immunochemically with the HPTLC-overlay method using anti-paragloboside (nLcOse$_4$) monoclonal antibody (kindly provided by Dr. Tai) after treatment with *Arthrobacter ureafaciens* neuraminidase (40 mU/ml) for 2 hr at room temperature. The amounts of ganglio-*N*-tetraosyl gangliosides other than GM3 were below the detection limit of the resorcinol-HCl reagent. The HPTLC plate was therefore developed with solvent system I and bands were incubated with *A. ureafaciens* neuraminidase (40 mU/ml) for 2 hr at room temperature and then overlaid with anti-rabbit asialo GM1 antibody (diluted 1:25) for 2 hr to detect these minor ganglio-*N*-tetraosyl species (Saito et al., 1985).

Quantitation of Neutral GSLs

The presence of Gb3 and Gb4 was confirmed using anti-Gb3 and anti-Gb4 monoclonal antibodies (kindly provided

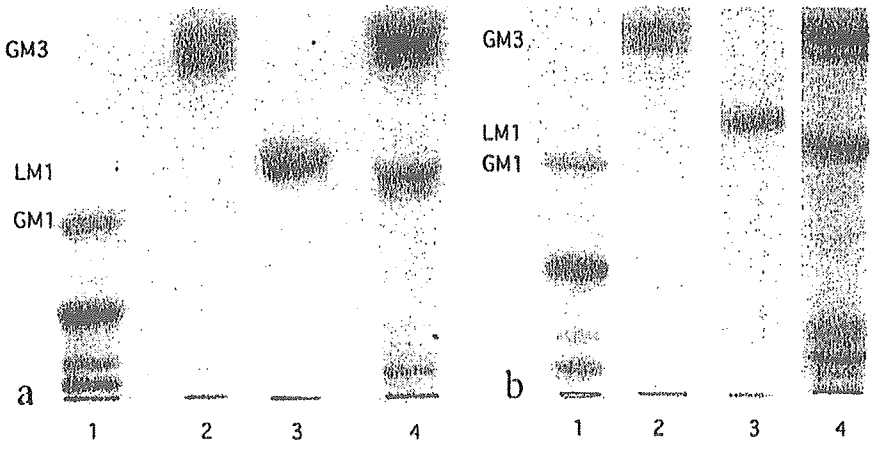

Fig. 1. Acidic glycosphingolipid (GSL) fraction in HUVECs (a) and HBMEC (b). Lane 1, human brain ganglioside standards (5 μg); lane 2, 1 μg of standard GM3 (NeuAc); lane 3, 1 μg of standard LM1; lane 4, acidic GSL fraction obtained from HUVECs (a) and HBMECs (b). The bands were visualized with the resorcinol-HCl reagent.

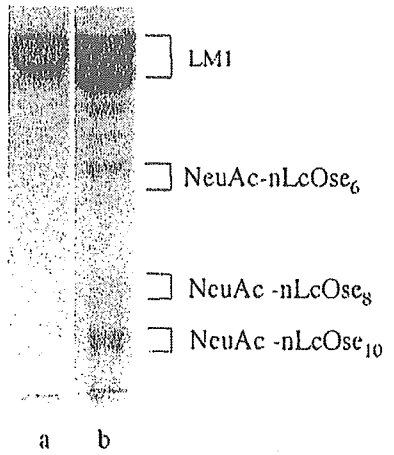

Fig. 2. a: Standard LM1 (1 μg). b: HPTLC-overlay method of acidic GSL fraction in HBMECs with the anti- nLcOse$_4$ monoclonal antibody after treatment with *A. ureafaciens* neuraminidase.

by Dr. Tai). The content of LacCer, Gb3, and Gb4 was determined by densitometric scanning of the chromatographic plate with comigration of authentic LacCer, Gb3, and Gb4, followed by visualizing with orcinol-sulfuric acid reagent.

Quantitation of SGPG (HPTLC-Overlay Method With Anti-SGPG Antibody)

Quantitative analysis of SGPG was achieved by the method described previously (Kanda et al., 1994). After the GSL fraction (collected from approximately 8–20-mg protein sample) and authentic SGPG (from 2–120 ng in quantity) were chromatographed in solvent system I, the plate was dipped in 0.4% polyisobutylmethacrylate solution in hexane for 1 min and air-dried. The plate was then incubated with LT serum (anti-SGPG antibody; immunoglobulin [Ig]M) for 2 hr, the serum from a patient with demyelinative neuropathy and IgM paraproteinemia that recognizes HNK-1 epitope, at a dilution of 1:1,000 in dilution buffer, followed by peroxidase conjugated rabbit anti-human IgM (μ-chain specific, 1:1,000; Cappel) for 2 hr. The LT serum (anti-SGPG antibody) was a generous gift from Dr. R.K. Yu (Department of Biochemistry and Molecular Biology, Institute of Molecular Medicine and Genetics, Medical College of Georgia, Augusta, GA). After washing with PBS, the plate was visualized with a Konica Immunostaining HRP 1000 (Konica, Seikagaku-kogyo, Japan). Although LT serum can react with SGPG, sulfoglucuronosyl lactosaminyl paragloboside (SGLPG) and band X (Ariga et al., 1987), only SGPG could be detected in HBMECs and HUVECs. SGPG was quantitated based on standard curves generated by densitometric scanning of known amounts of SGPG developed on the same plate.

Immunostaining of HBMECs and HUVECs With Anti-SGPG Antibody

Confluently or nonconfluently cultured HBMECs and HUVECs on collagen type I-coated glass slides were fixed with 4% paraformaldehyde for 15 min and washed with PBS at least three times. After incubation in PBS with 3% nonimmunized rabbit serum, LT serum (anti-SGPG antibody; diluted 1:100 in PBS) was applied at 4°C for 72 hr. The slides were washed three times and fluorescein isothiocyanate (FITC)-conjugated rabbit anti-human IgM (μ-chain specific, 1:1,000; Cappel) was applied for 1 hr at room temperature.

HPTLC/Matrix-Assisted Secondary Ion Mass Spectrometry

Negative secondary ion mass spectrometry (SIMS) spectra of GSLs were recorded on a Finnigan TSQ 70 quadrupole mass spectrometer in the negative ion mode equipped with a cesium ion (Cs) gun as follows. After developing GSLs on an HPTLC plate, a primuline reagent was sprayed over the plate until it is visibly wet GSLs on the plate were viewed under UV light at 380 nm. Each GSL band was marked with a colored drawing pencil while still under illumination. The plate was then immersed for 20 sec in a solvent composed of 2-propanol:methanol:0.2% aqueous $CaCl_2$ (40:20:7, vol/vol). It was then placed on another glass plate, after which a polyvinylidene difluoride (PVDF) membrane sheet and a glass microfilter sheet were

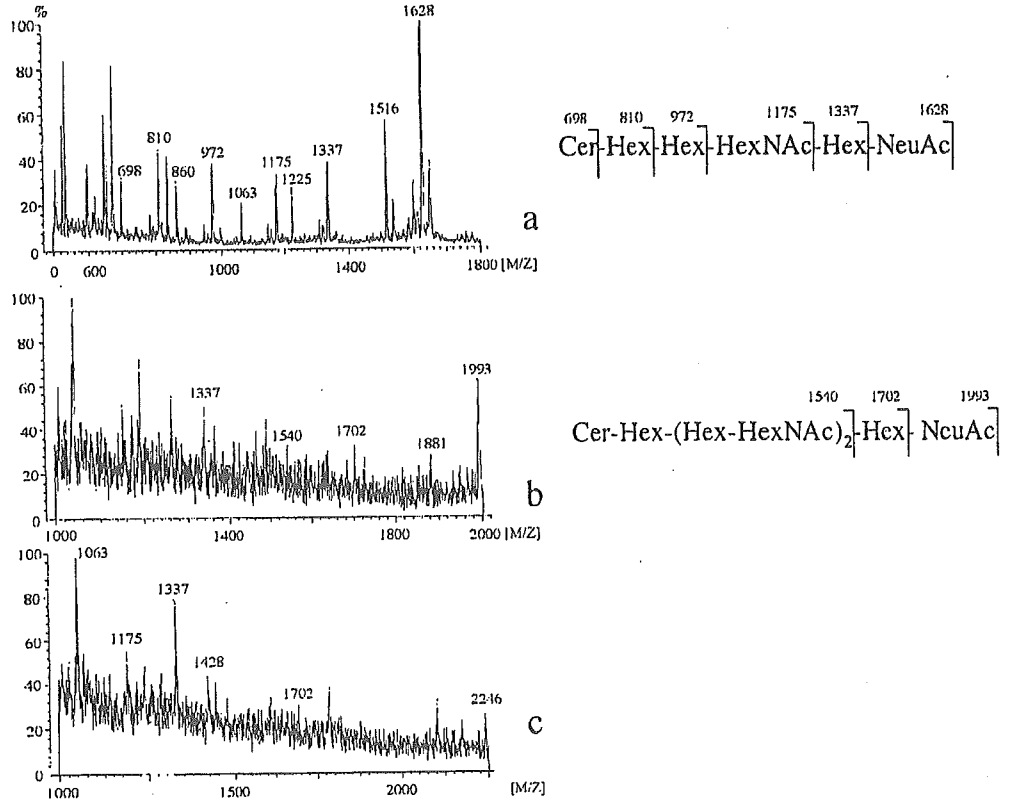

Fig. 3. Mass spectrometry of LM1 (a), NeuAc-nLcOse$_6$ (b), and NeuAc-nLcOse$_8$ (c) from HBMECs.

placed over the plate. The "sandwich" was then pressed with a household iron (about 180°C) for 30 sec. The PVDF membrane was separated from the HPTLC plate, washed with water to remove the primuline reagent, and then dried. The GSL band on the PVDF membrane was excised (2 mm in diameter) and placed on a mass spectrometer prove tip, and few microliters of triethanolamine was added as the matrix. Samples on the membrane were bombarded with a Cs^+ beam at 20 kV. The ion multiplier was kept at 1.5 kV and the conversion dynode at 20 kV (Ishikawa et al., 1995; Taki et al., 1995).

RESULTS

Glycosphingolipid composition of cultured HBMECs and HUVECs are shown in Table I.

Ganglioside Composition in HBMECs

Figure 1 shows the ganglioside pattern of the HBMECs. The two major gangliosides were identified as GM3 (NeuAc) and sialyl paragloboside (LM1; NeuAc-nLcOse$_4$) using authentic samples of GM3 (NeuAc) and LM1. LM1 was identified by HPTLC-overlay method using anti-paragloboside monoclonal antibody after neuraminidase treatment (see Fig. 2). Most bands observed in polysialoganglioside regions (Fig. 1a,b; lane 4) are neolacto-*N*-tetraose series gangliosides; it was impossible to detect ganglio-*N*-tetraose series gangliosides using resorcinol-sulfuric acid reagent (Kanda et al., 1994). In addition, this method revealed that acidic GSL fraction contained several gangliosides containing paragloboside core structures (lacto-*N*-tetraose series gangliosides; Fig. 2). The structures of these gangliosides were confirmed by HPTLC/matrix-assisted SIMS (Ishikawa et al., 1995; Taki et al., 1995) as shown in Figure 3. Negative SIMS mass spectra of gangliosides can provide information on their molecular weights and sugar sequences as well as their fatty acid and long chain base compositions. The mass spectra revealed prominent deprotonated molecules $[M - H]^-$, which corresponded to GSL molecular species containing fatty acids with chain lengths ranging from C18:0 to C24:0 and C18 sphingenine. The band comigrating to LM1 was ceramide (Cer) pentasaccharide that was found to be Cer (m/e 536-m/z 648), Cer-Hex (m/z 698-m/z 810), Cer-Hex-Hex (m/z 860-m/z 972), Cer-Hex-Hex-HexNAc (m/z 1063-m/z 1175), Cer-Hex-Hex-HexNAc-Hex (m/z 1225-m/z 1337) and Cer-Hex-Hex-HexNAc-Hex-NeuAc ($[M - H]^-$; m/z 1517-m/z 1629) (Fig. 3a). The lower band of LM1 that reacted with

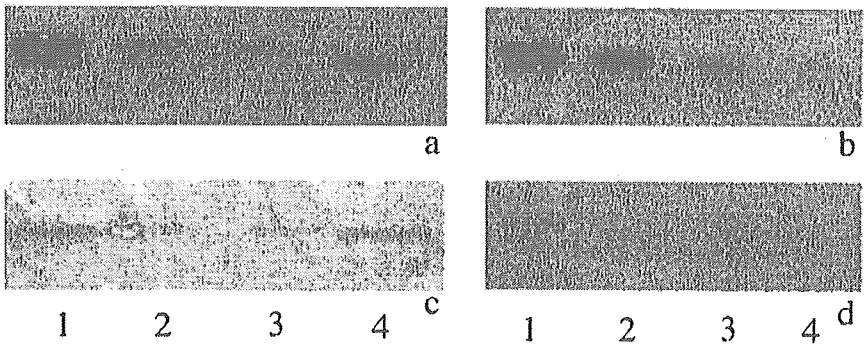

Fig. 4. HPTLC-overlay method of SGPG at a nonconfluent state in HUVECs (a) and HBMECs (c) and after confluency in HUVECs (b) and HBMECs (d). Lanes 1–3: 1.6, 0.8, and 0.4 ng of standard SGPG, respectively. Lane 4: in (a), acidic GSL fraction from 0.05 mg protein of HUVECs at nonconfluent state; in (b), acidic GSL fraction from 0.5 mg protein of HUVECs after confluency; in (c), acidic GSL fraction from 1 mg protein of HBMECs at a nonconfluent state; and in (d), acidic GSL fraction from 1 mg protein in HBMECs after confluency.

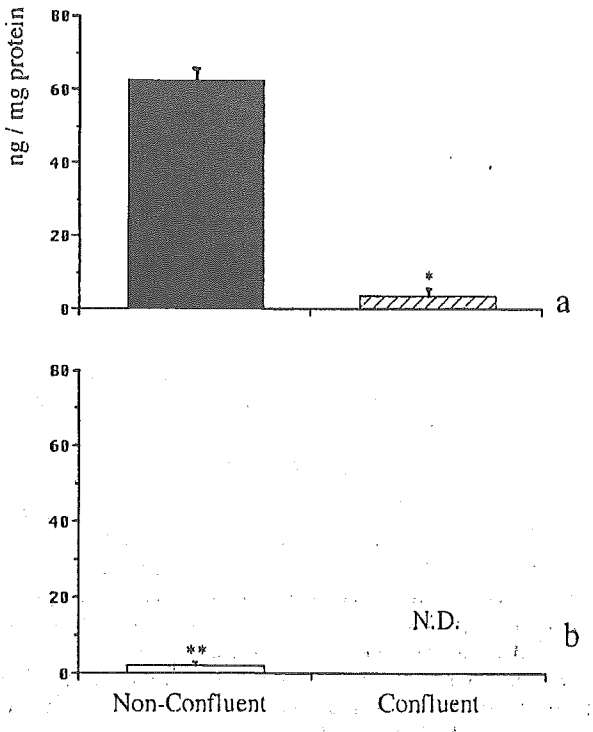

Fig. 5. SGPG content in HUVECs (a) and HBMECs (b) at nonconfluent state and after confluency. $n = 3$. Bars denote SEM. $*P < 0.0001$; $**P < 0.001$ vs. HUVECs at a nonconfluent state (black bar).

anti-paragloboside monoclonal antibody showed the deprotonated molecules (m/z 1516-m/z 1628), suggesting the presence of positional isomer of LM1 containing NeuAc (2→6) (data not shown), which the structure of NeuAc (2→6)-nLcOse$_4$ was reported by several investigators (Fukuda et al., 1985; Nojiri et al., 1988). The band that migrated to the middle position was Cer-heptasaccharide, which was found to be Cer-Hex-Hex-HexNAc-Hex (m/z 1225-m/z 1337), Cer-Hex-Hex-HexNAc-Hex-HexNAc (m/z 1428-m/z 1540), Cer-Hex-Hex-HexNAc-Hex-HexNAc-Hex (m/z 1590-m/z 1702), and Cer-Hex-Hex-HexNAc-Hex-HexNAc-Hex-NeuAc ([M - H]$^-$; m/z 1881-m/z 1993) (Fig. 3b). The second band migrated from the bottom was supposed to be Cer-nonasaccharide, but was found to be Cer-Hex-Hex-HexNAc-Hex (m/z 1225-m/z 1337), Cer-Hex-Hex-HexNAx-Hex-HexNAc (m/z 1428), Cer-Hex-Hex-HexNAc-Hex-HexNAc-Hex (m/z 1702), and Cer-Hex-Hex-HexNAc-Hex-HexNAc-Hex-HexNAc-Hex-NeuAc ([M - H]$^-$; m/z 2246) containing C18:0 fatty acid and sphingenine. Unfortunately, the deprotonated molecule at m/z 2359 containing C24:0 fatty acid and sphingenine was not detected because it was out of scales. The lower band reacted with anti-paragloboside monoclonal antibody may be ceramide containing 11 saccharides because several ions containing background ions were detected in near the deprotonated molecules (m/z 2612 - m/z 2724; data not shown). In HBMECs, GM3 and LM1 increased significantly after confluency ($P < 0.05$ and $P < 0.01$, respectively). Four ganglio-*N*-tetraosyl gangliosides, including GM1, GD1a, GD1b, and GT1b, were also detected in HUVECs and HBMECs as minor species using *A. ureafaciens* neuraminidase and anti-asialo GM1 antibody (Saito et al., 1985). No appreciable difference was noted, however, in their compositions before and after confluency.

SGPG in HBMECs and HUVECs

SGPG was found in the GSL fraction of HBMECs and HUVECs by the HPTLC-immunostaining method (Fig. 4). Neither SGLPG nor band X, found previously in human peripheral nerve (Kohriyama et al., 1987), could be detected by this method. The latter was identified as

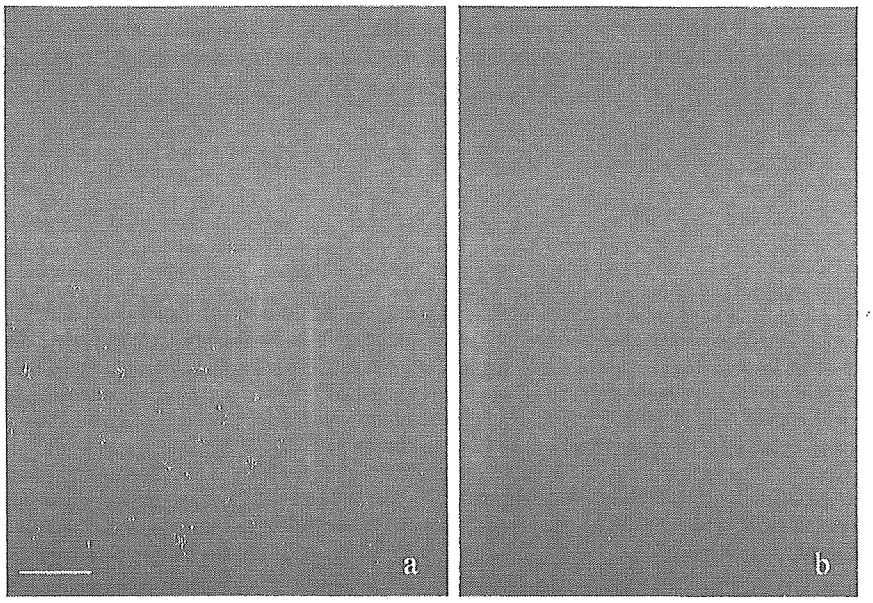

Fig. 6. Immunostaining of HUVECs before (a) and after (b) confluency using LT serum (anti-SGPG antibody). In HBMECs, no appreciable immunofluorescence was detected (data not shown). Scale bar = 100 μm.

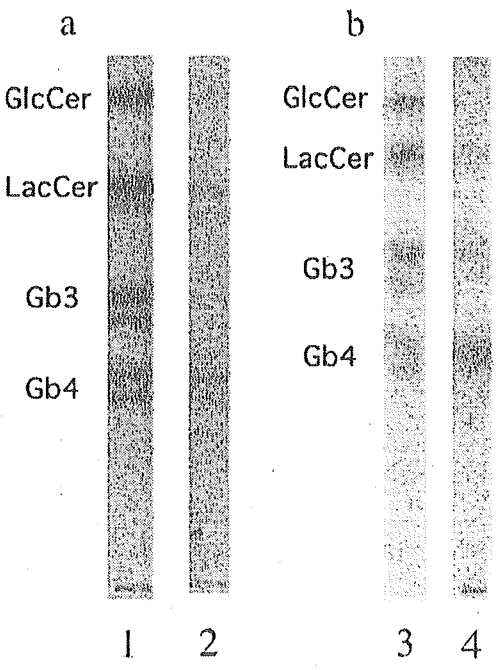

Fig. 7. Thin-layer chromatogram of neutral GSLs in HUVEC (a) and HBMEC (b). Lanes 1 and 3: 1 μg each of authentic GlcCer from human brain, LacCer, Gb3, Gb4 from porcine erythrocyte membranes (from top to bottom). Lane 2: neutral GSL fraction from HUVECs. Lane 4: neutral GSL fraction from HBMECs.

lysophosphatidylinositol (Suzuki et al., 2001). Figure 5 shows the quantitative difference of SGPG in HBMECs and HUVECs, at confluent as well as at nonconfluent culture phases. Under the nonconfluent condition, especially, when endothelial cells are in the proliferation phase and cell-to-cell contact is not conspicuous, the SGPG content in HUVECs was more than forty times as abundant as that in HBMECs. After confluency, the SGPG content in HUVECs was decreased (1/30) and no SGPG was detected in confluent HBMECs (Fig. 6).

Neutral GSL Composition of HBMECs

GSL structures were verified by immunostaining with specific anti-neutral GSL antibodies on thin-layer chromatograms. Figure 7 shows the orcinol-stained HPTLC pattern of the neutral GSL fraction in HBMECs and HUVECs, indicating these endothelial cells comprise three major neutral GSLs including LacCer, Gb3, and Gb4. The structures of these neutral GSLs were confirmed by HPTLC/SIMS (data not shown) and the HPTLC-GSL overlay method using specific antibodies (Fig. 8). Negative SIMS mass spectra of neutral GLSs showed prominent dehydrogenated molecular ions $[M - H]^-$ that corresponded to GSL molecular species containing fatty acids with chain lengths ranging from C18:0 to C24:0 and C18 sphingenine. The band comigrating to LacCer showed the fragmented ions corresponding to ceramide (Cer) (m/z 536-m/z 648), Cer-monosaccharide (m/z 698-m/z 810), and Cer-disaccharide ($[M - H]^-$; m/z 860-m/z 972), resulting in Cer-Hex-Hex. The lower two bands showed the same fragment ions corresponding to Cer, Cer-monosaccharide, and Cer-disaccharide. In the band comigrating to Gb3, the terminal sugar was found to be hexose (Hex) (m/z 162), resulting in Cer-Hex-Hex-Hex ([M -

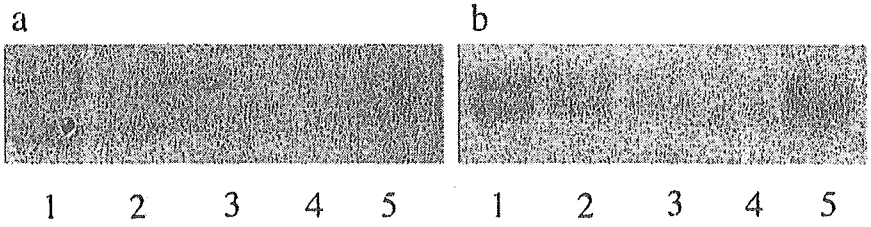

Fig. 8. HPTLC-overlay method with anti-Gb3 antibody (a) and anti-Gb4 antibody (b). Lanes 1–4: 1, .5, 0.1, 0.05 μg of authentic Gb3 (a) and Gb4 (b), respectively. Lane 5: neutral GSL fraction obtained from confluent HUVECs.

$H]^-$; m/z 1134). The band comigrating to Gb4 was Cer-tetrasaccharide and terminal sugar found to be *N*-acetylhexosamine (HexNAc) (m/z 203), resulting in Cer-Hex-Hex-Hex-HexNAc ($[M - H]^-$; m/z 1225-m/z 1337). Neither HBMECs nor HUVECs contained glucosyl ceramide or galactosyl ceramide, so far as HPTLC pattern. The amount of Gb3 in HBMECs was almost as twice that in HUVECs. No appreciable differences in neutral GSL quantity were observed before and after confluency.

DISCUSSION

It is difficult to guarantee that the cultured brain-derived ECs are really originated from ECs forming BBB. Such an assumption is made usually from elongated, fibroblast-like shape or increased resistance and limited passage of small molecules through monolayer of these cells, but conventional methods to isolate BMECs cannot escape contamination of ECs other than BMECs, namely, ECs from larger vessels lacking BBB properties. To solve this problem, we first carried out DNA microarray analysis to confirm expression of one of the most important barrier-specific genes, *mdr1* (Cordon-Cardo et al., 1989), in ECs used in the present study. Because we confirmed *mdr1* gene expression in HBMECs and its absence in HUVECs, the GSL content differences in HBMECs and HUVECs may partially reflect possible differences in cellular properties related to BBB function.

The most striking difference between GSL content of HBMECs and HUVECs is the amount of SGPG. This HNK-1 epitope-bearing GSL belongs to a novel class of acidic lipids present primarily in peripheral nerve tissues (Chou et al., 1986; Ariga et al., 1987). In mammalian CNS, sulfoglucuronosyl GSLs (SGGLs) including SGPG are known to be developmentally regulated, being expressed in embryonic forebrain and disappearing during the postnatal period (Schwarting et al., 1987), except in murine cerebellum (Chou and Jungalwala, 1988) and human optic nerve (Yoshino et al., 1993). Other than CNS parenchyma, we provided evidence that SGPG is an integral component of cultured bovine BMECs and demonstrated that SGPG is the only GSL whose concentration shows a wide fluctuation depending upon culture conditions and age (Kanda et al., 1994). Treatment of these cells with interleukin 1β (IL-1β) induced accumulation of SGPG (Kanda et al., 1995). In the present study, we found SGPG in HBMECs was much lower than that in HUVECs, and the SGPG content in both cells decreased markedly after confluency. Such marked fluctuations in SGPG expression, influenced by culture age, inflammatory cytokines, and the presence or absence of contact inhibition, may suggest a functional importance of this GSL as the surface receptor of ECs forming the BBB.

These changes in expression of SGPG may be due primarily to rapid upregulation and downregulation of glucuronyltransferase activity, probably triggered by endothelial cell–endothelial cell contact. COS-1 cells transfected with glucuronyltransferase-P cDNA (an enzyme involved in the biosynthesis of the HNK-1 epitope) (Seiki et al., 1999) and transformed into HNK-1-positive cells lost the tendency to aggregate and remained single cells (Kawasaki and Oka, 2001). The previous data and our findings indicate that the HNK-1 epitope, also known as an adhesion molecule, inhibits homophilic contact between HNK-1 epitope-bearing cells and is expressed mainly in single, proliferating cells. Because SGPG localized on BMECs acts as ligand for L-selectin expressed on the surface of circulating lymphocytes (Kanda et al., 1995) and anti-SGPG antibody (LT serum) possibly reacts with ECs forming the blood–nerve barrier and impairs their barrier function (Kanda et al., 1994, 1998), SGPG-rich proliferating ECs that repair injured barrier system may have more chance to be attacked by lymphocytes and antibodies; thus forming a vicious circle of inflammation.

The amounts of two major acidic GSLs, GM3 (NeuAc) and LM1, was also smaller in HBMECs than in HUVECs. Different from that of SGPG, the amount of GM3 (NeuAc) and LM1 was increased significantly after confluency in HBMECs. Neutral GSLs did not show any significant changes after confluency. The physiologic meaning of this difference is unknown; however, these dynamic changes in amounts of acidic GSLs including SGPG may be based on signaling systems triggered by endothelial cell–endothelial cell contact and might influence BBB integrity. The presence of neolacto-series gangliosides including NeuAc-nLcOse$_6$, NeuAc-nLcOse$_8$, and NeuAc-nLcOse$_{10}$ in HBMECs and HUVECs (Muthing et al., 1999) was confirmed using the HPTLC-overlay method and Far-Eastern blot/mass spectrometry. These minor species, however, did not show any difference between HUVECs and HBMECs.

Finally, the differences in GSL content observed in the present study and reported in previous studies are briefly discussed. HBMECs express a composition of

acidic GSLs similar to that reported previously for primary ECs from various sources (Kanda et al., 1994, 1997) and for immortalized human brain ECs (Duvar et al., 2000). The amount of acidic GSLs, however, is smaller than that observed in bovine BMECs (Kanda et al., 1994) and in immortalized human brain ECs (Duvar et al., 2000). The difference is more conspicuous in neutral GSLs: HBMEC comprise Gb4, Gb3, and LacCer as major constituents of neutral GSL whereas only GlcCer was detected in bovine BMECs (Kanda et al., 1994). These variations in expression might be attributable to species specificity and to SV40 T-antigen immortalization of ECs. Our data obtained from primary culture of nontransformed HBMECs thus should reflect more closely the in vivo GSL content of endothelial cells forming the BBB.

Species differences in neutral GSLs was also demonstrated in this study. Gb3 is known as the specific receptor for verotoxin that has been implicated strongly as the causative agent for most cases of postdiarrheal hemolytic uremic syndrome (HUS) (Lingwood, 1996) and the difference of Gb3 expression level in each organ might lead to attack of a specific organ. In this regard, preferential involvement of kidney in HUS can be well explained because verotoxin is considered to target the Gb3-rich renal microvasculature (Obrig et al., 1993) resulting in renal disorder. No reasonable explanation has ever been provided, however, for the CNS tropism in HUS. We demonstrated that the amount of Gb3 is approximately twice as abundant in HBMECs compared to that in HUVECs. This endothelial heterogeneity may explain the frequent involvement of CNS in this disorder.

ACKNOWLEDGMENT

We thank Dr. T. Tai (Department of Tumor Immunology, The Tokyo Metropolitan Institute of Medical Science) for kindly providing anti-Gb3, anti-Gb4, and anti-paragloboside monoclonal antibodies.

REFERENCES

Ando S, Chang NC, Yu RK. 1978. High-performance thin-layer chromatography and densitometric determination of brain ganglioside composition of several species. Ann Biochem 89:437–450.

Ariga T, Kohriyama T, Freddo L, Latov N, Saito M, Kohn K, Ando S, Suzuki M, Hemling ME, Rinehart KL, Kusunoki S, Yu RK. 1987. Characterization of sulfate glucuronic acid containing glycolipids reacting with IgM-M proteins in patients with neuropathy. J Biol Chem 262:848–853.

Bradford MM. 1976. A rapid and sensitive method for the quantification of protein utilizing the principle of protein-dye binding. Anal Biochem 72:248–254.

Chou DK, Ilyas AA, Evans JE, Costello C, Quarles RH, Jungalwala FB. 1986. Structure of sulfated glycolipids in the nervous system reacting with HNK-1 antibody and some IgM paraprotein in neuropathy. J Biol Chem 261:11717–11725.

Chou DK, Jungalwala FB. 1988. Sulfoglucuronyl neolactoglycolipids in adult cerebellum: specific absence in murine mutants with Purkinje cell abnormality. J Neurochem 50:1655–1658.

Cordon-Cardo C, O'Brien JP, Casals D, Rittman-Grauer L, Biedler JL, Melamed MR, Bertino JR. 1989. Multidrug-resistance gene (P-glycoprotein) is expressed by endothelial cells at blood-brain barrier. Proc Natl Acad Sci USA 86:695–698.

Duvar S, Suzuki M, Muruganandam A, Yu RK. 2000. Glycosphingolpid composition of a new immortalized human cerebromicrovascular endothelial cell line. J Neurochem 75:1970–1976.

Fukuda MN, Dell A, Oates JE, Wu P, Klock JC, Fukuda M. 1985. Structures of glycosphingolipids isolated from human granulocytes. J Biol Chem 260:1067–1082.

Gordon EL, Danielsson PE, Nguyen T, Winn HR. 1991. A comparison of primary cultures of rat cerebral microvascular endothelial cells to rat aortic endothelial cells. In Vitro Cell Dev Biol 27:313–326.

Handa S. 1963. Blood group active glycolipid from human erythrocytes. Jpn J Exp Med 33:347–360.

Ishikawa D, Kato T, Handa S, Taki T. 1995. New methods using polyvinylidene difluoride membranes to detect enzymes involved in glycosphingolipid metabolism. Anal Biochem 231:13–19.

Jaffe EA. 1987. Cell biology of endothelial cells. Hum Pathol 18:234–239.

Kanda T, Iwasaki T, Yamakawa T, Ikeda K. 1997. Isolation and culture of bovine endothelial cells of endoneurial origin. J Neurosci Res 49:769–777.

Kanda T, Usui S, Beppu H, Miyamoto K, Yamawaki M, Oda M. 1998. Blood-nerve barrier in IgM paraproteinemic neuropathy: a clinicopathologic assessment. Acta Neuropathol (Berl) 95:184–192.

Kanda T, Yamawaki M, Ariga T, Yu RK. 1995. Interleukin-1 beta upregulates the expression of sulfoglucuronosyl paragloboside, a ligand for L-selectin, in brain microvascular endothelial cells. Proc Natl Acad Sci USA 92:7897–7901.

Kanda T, Yoshino H, Ariga T, Yamawaki M, Yu RK. 1994. Glycosphingolipid antigens in cultured microvascular bovine brain endothelial cells: sulfoglucuronyl paragloboside as a target of monoclonal IgM in demyelinative neuropathy. J Cell Biol 126:235–246.

Karlsson KA. 1995. Microbial recognition of target-cell glycoconjugates. Curr Opin Struct Biol 5:622–635.

Kawasaki T, Oka S. 2001. [Roles of the HNK-1 carbohydrate epitope in the nervous system.] Nihon Shinkei Seishin Yakurigaku Zasshi 21:95–99.

Kohriyama T, Kusunoki S, Ariga T, Yoshino JE, DeVries GH, Latov N, Yu RK. 1987. Subcellular localization of sulfated glucuronic acid-containing glycolipids reacting anti myelin-associated glycoprotein antibody. J Neurochem 48:1516–1522.

Lingwood CA. 1996. Role of verotoxin receptors in pathogenesis. Trends Microbiol 4:147–153.

Muthing J, Duvar S, Heitmann D, Hanisch HG, Neumann U, Lochnit G, Geyer R, Peter-Katalinic J. 1999. Isolation and structural characterization of glycosphingolipids of in vitro propagated human umbilical vein endothelial cells. Glycobiology 9:459–468.

Nojiri H, Kitagawa S, Nakamura M, Kirito K, Enomoto Y, Saito M. 1988. Neolacto-series gangliosides induce granulocytic differentiation of human promyelocytic leukemia cell line HL-60. J Biol Chem 263:7443–7446.

Obrig TG, Louise CB, Lingwood CA, Boyd B, Barley-Maloney L, Daniel TO. 1993. Endothelial heterogeneity in Shiga toxin receptors and responses. J Biol Chem 268:15484–15488.

Riboni L, Viani P, Bassi R, Prinetti A, Tettamanti G. 1997. The role of sphingolipids in the process of signal transduction. Prog Lipid Res 36: 153–195.

Saito M, Kasai N, Yu RK. 1985. In situ immunological determination of basic carbohydrate structure of gangliosides on thin-layer plates. Anal Biochem 148:54–58.

Schwarting GA, Jungalwala FB, Chou DKH, Boyer AM, Yamamoto M. 1987. Glucuronic acid and sulfate containing glycoconjugates are temporally and spatially regulated antigens in the developing mammalian central nervous system. Dev Biol 120:65–76.

Seiki T, Oka S, Terayama K, Imiya K, Kawasaki T. 1999. Molecular cloning and expression of a second glucuronyltransferase involved in the biosynthesis of the HNK-1 carbohydrate epitope. Biochem Biophys Res Commun 255:182–187.

Sekine M, Ariga T, Miyatake T, Kuroda Y, Suzuki A, Yamakawa T. 1984. Ganglioside composition of chromaffin granule membrane in bovine adrenal medulla. J Biochem (Tokyo) 95:155–160.

Suzuki M, Suetake K, Kasama T, Ariga T, Shiina M, Kusunoki S, Yu RK. 2001. Characterization of a phospholipid antigen reacting with serum antibody in patients with peripheral neuropathies and paraproteinemia. J Neurochem 79:970–975.

Svennerholm L. 1964. The gangliosides. J Lipid Res 5:145–153.

Taki T, Ishikawa D, Handa S, Kasama T. 1995. Direct mass spectrometric analysis of glycosphingolipid transferred to a polyvinylidene difluoride membrane by thin-layer chromatography blotting. Anal Biochem 225: 24–27.

Voyta JC, Via DP, Butterfield CE, Zetter BR. 1984. Identification and isolation of endothelial cells based on their increased uptake of acetylated-low density lipoprotein. J Cell Biol 99:2034–2040.

Yoshino H, Maeda Y, King M, Cartwright MJ, Richards DW, Ariga T, Yu RK. 1993. Sulfated glucuronyl glycolipids and gangliosides in the optic nerve of humans. Neurology 43:408–411.

Yu RK, Yoshino H, Yamawaki M, Yoshino JE, Ariga T. 1994. Subcellular distribution of sulfated glucuronyl glycolipids in human peripheral motor and sensory nerves. J Biomed Sci 1:167–171.

International Immunology, Vol. 17, No. 12, pp. 1619–1629
doi:10.1093/intimm/dxh342

Preferential T_h2 polarization by OCH is supported by incompetent NKT cell induction of CD40L and following production of inflammatory cytokines by bystander cells *in vivo*

Shinji Oki, Chiharu Tomi, Takashi Yamamura and **Sachiko Miyake**

Department of Immunology, National Institute of Neuroscience, NCNP, 4-1-1 Ogawahigashi, Kodaira, Tokyo 187-8502, Japan

Keywords: cell activation, cytokines, inflammation, natural killer, rodent, T cells

Abstract

The altered glycolipid ligand OCH is a selective inducer of T_h2 cytokines from NKT cells and a potent therapeutic reagent for T_h1-mediated autoimmune diseases. Although we have previously shown the intrinsic molecular mechanism of preferential IL-4 production by OCH-stimulated NKT cells, little is known about the extrinsic regulatory network for IFN-γ production. Here we demonstrate that OCH induces lower production of IFN-γ, not only by NKT cells but also by NK cells compared with α-galactosylceramide. OCH induced lower IL-12 production due to ineffective primary IFN-γ and CD40 ligand expression by NKT cells, and resulted in lower secondary IFN-γ induction. Co-injection of a sub-optimal dose of IFN-γ and stimulatory anti-CD40 mAb compensates for the lower induction of IL-12 by OCH administration. IL-12 converts OCH-induced cytokine expression from IL-4 predominance to IFN-γ predominance. Furthermore, CpG oligodeoxynucleotide augmented IL-12 production when co-administrated with OCH, resulting in increased IFN-γ production. Taken together, the lower IL-12 production and subsequent lack of secondary IFN-γ burst support the effective T_h2 polarization of T cells by OCH. In addition, highlighted in this study is the characteristic property of OCH that can induce the differential production of IFN-γ or IL-4 according to the availability of IL-12.

Introduction

NKT cells are a unique subset of CD1d-restricted T lymphocytes that express TCR and some NKR. NKT cells recognize glycolipid antigens such as α-galactosylceramide (αGC) by an invariant TCRα chain composed of Vα14-Jα18 segments in mice and Vα24-Jα18 segments in humans, associated with TCRβ chains using a restricted set of Vβ genes (1, 2). NKT cells rapidly secrete large amounts of cytokines including IL-4 and IFN-γ upon antigen stimulation and are effective regulators of T_h1/T_h2 balance *in vivo* (3–5). We have previously demonstrated that *in vivo* administration to mice of altered glycolipid ligand, OCH, ameliorates experimental autoimmune encephalomyelitis (EAE), collagen-induced arthritis (CIA) and type I diabetes by enhancing IL-4-dependent T_h2 responses without inducing IFN-γ production and pathogenic T_h1 responses (6–8).

Recently, we have clarified the intrinsic molecular mechanism of preferential IL-4 production by OCH-stimulated NKT cells (9). IFN-γ production by NKT cells was more susceptible to the sphingosine length of glycolipid ligand than that of IL-4, and the length of sphingosine chain determined the half-life of NKT cell stimulation by CD1d-associated glycolipids. IFN-γ production by NKT cells required longer T cell stimulation than did IL-4 production and the transcription of the IFN-γ gene required *de novo* protein synthesis by activated NKT cells. The NF-κB family member transcription factor c-Rel was preferentially transcribed in αGC-stimulated, but not in OCH-stimulated, NKT cells and was identified as essential for IFN-γ production by activated NKT cells. Therefore, the differential duration of NKT cell stimulation, due to the binding stability of individual glycolipid antigens to CD1d molecules, determines whether signaling leads to effective c-Rel transcription and IFN-γ production by activated NKT cells.

Upon stimulation by αGC *in vivo*, NKT cells rapidly affect the functions of neighboring cell populations such as T cells, NK cells, B cells and dendritic cells (DCs) in a direct or indirect manner (10–13). The serial production of IFN-γ by NKT cells

Correspondence to: S. Miyake; E-mail: miyake@ncnp.go.jp

Transmitting editor: K. Okumura

Received 19 August 2005, *accepted* 30 September 2005

Advance Access publication 15 November 2005